



Regular Paper

A 9-year study of the degradation of a HDPE geomembrane liner used in different high pH mining applications

Rodrigo A. e Silva^a, Fady B. Abdelaal^a, R. Kerry Rowe^{b,*}

^a GeoEngineering Centre at Queen's-RMC, Queen's University, Ellis Hall, Kingston ON, K7L 3N6, Canada

^b Geotechnical and Geoenvironmental Engineering, GeoEngineering Centre at Queen's-RMC, Queen's University, Ellis Hall, Kingston ON, K7L 3N6, Canada



ARTICLE INFO

Keywords:

Geosynthetics
Geomembrane
Mining
Heap leaching
Degradation
Nominal failure
Arrhenius

ABSTRACT

The degradation of a HDPE geomembrane in heap leaching environments is evaluated using immersion tests at five temperatures. The incubation solutions had a pH of 9.5, 11.5, and 13.5, relevant to gold and silver pregnant liquor solutions. After 9.3 years, the geomembrane's mechanical properties had reached nominal failure at 95, 85, and 75 °C in all three solutions. It is shown that the pH 13.5 solution had the greatest effect on the anti-oxidant depletion (Stage I) and polymer degradation (Stage III), but was the least aggressive to initiate the degradation (Stage II) compared to the pH 11.5 and 9.5 solutions. Overall, the time to nominal failure (time to 50% of the initial or specified property value) in pH 13.5 was slightly shorter than the pH 9.5 and 11.5 solutions. Based purely on immersion tests, the time to nominal failure of this specific geomembrane at 30 °C is predicted to be 150 years in the pH 9.5 and 11.5 solutions, and 140 years in the pH 13.5 solution. Assuming a good liner design that limits the tensile strains in the GMB, nominal failure in a composite liner configuration is predicted to exceed 260 years at 30 °C and the expected value could exceed 1000 years at 10 °C.

1. Introduction and background

Heap leaching is one of several hydrometallurgical technologies for treating precious-metal ores, and is often selected due to its low capital cost relative to alternative approaches such as gravity concentration, flotation and agitated tank-leaching (Pyper et al., 2019). The process involves stacking metal-bearing ore into heaps on an impermeable liner and irrigating it with a lixiviant (generally known as the raffinate) that percolates through the ore (Petersen 2016; Robertson et al., 2022). The metal-rich 'pregnant' leach solution (PLS) is then collected at the bottom of the heap and the target metals are subsequently recovered.

Various types of heap leach pads are available, including permanent single-lift and multi-lift heaps, dynamic heaps (also known as on-off heaps), and valley-fill heaps (Thiel and Smith 2004). A common feature across these configurations is the liner system that is typically designed using geosynthetic materials to preserve the PLS and to minimize its release to the environment. Single or occasionally double composite liner systems are used (Lupo 2010). A single composite liner consists of a geomembrane (GMB) layer placed over compacted liner bedding soil (Rowe et al., 2004). This configuration may be suitable for areas with low hydraulic heads or where the subgrade has relatively low

permeability, such as in single-lift heaps (Lupo and Morrison 2007). Double composite liners include two GMB layers separated by a leak collection/drainage layer (Rowe et al., 2004). These are more suitable for high hydraulic heads, as is generally the case with valley leach facilities (Lupo 2010; Pries et al., 2014). For leach pads, solution ponds or runoff channels, high-density polyethylene (HDPE) is among the most commonly used GMB materials (Thiel and Smith 2004; Breitenbach and Smith 2006; Rowe et al., 2013; Ghorbani et al., 2016; Thenepalli et al., 2019; Lavoie et al., 2021; Abdelaal and Rowe 2023).

The GMB encounters harsh conditions during its service life, especially in the pad under the heaps. In addition to the significantly high overburden stresses, heap leaching involves exposure of the GMB to corrosive solutions. Particularly for gold and silver extraction, the HDPE GMBs are exposed to extremely high pH. This is because a dilute solution of sodium cyanide (pH of ~ 9.5–11) is used to dissolve gold/silver without dissolving other ore components such as copper, zinc and iron (Manning and Kappes 2016). Sodium hydroxide (NaOH) is typically added to maintain the desired alkalinity of the cyanide leaching system (Asamoah et al., 2018), as well as a pre-leaching step to enhance metal recovery (Espitia and Lapidus 2015; Snyders et al., 2018; Yang et al., 2021). Leaching at pH 12–13 to increase the rate of gold dissolution has

* Corresponding author.

E-mail addresses: r.esilva@queensu.ca (R.A. e Silva), fady.abdelaal@queensu.ca (F.B. Abdelaal), kerry.rowe@queensu.ca (R.K. Rowe).

also been reported as a common practice (Melashvili et al., 2016; Oraby and Eksteen 2016). When dealing with such a corrosive PLS, a primary concern is the potential chemical degradation of the GMB. Excessive degradation may lead to a shorter service life of the GMB liner, potentially compromising the desired design life of the heap leach facility.

HDPE GMB degradation has been conceptually divided into (Hsuan and Koerner 1998; Rowe and Sangam 2002): (a) the loss of antioxidants due to chemical consumption or physical extraction (Stage I); (b) induction time in which degradation in the polymer is initiated but is not sufficiently propagated to lead to a measurable degradation in properties such as stress-crack resistance (SCR), high-load melt flow index (HLMI) and tensile strength (Stage II); and (c) degradation to nominal failure (Stage III). Based on changes in tensile properties, nominal failure is reached when a particular property (e.g., break strength or elongation) decreases to 50% of its initial value (Hsuan and Koerner 1998), or 50% of the specified GRI-GM13 value (GRI 2021). For a GMB exhibiting physical ageing (Ewais and Rowe 2014; Rowe et al., 2019; Morsy and Rowe 2020), nominal failure based on SCR is typically defined as the point at which SCR decreases to 50% of the stabilized value after physical ageing (i.e., 50% of the so-called SCR_m value). The assessment of GMB degradation behaviour and chemical compatibility with liquids in the field can be investigated in the laboratory using oven immersion tests at various elevated temperatures, followed by Arrhenius modelling to extrapolate the degradation at specific field temperatures (ASTM D5322, 2023; Sangam and Rowe 2002; Jeon et al., 2008; Rowe et al., 2010; Abdelaal and Rowe 2014a; Abdelaal et al., 2015; Ewais et al., 2018; Abdelaal et al., 2019; Morsy and Rowe 2020; Li et al., 2021; Morsy et al., 2021; Clinton and Rowe 2023).

The assessment of the performance of GMBs in different mining applications using oven ageing has been considered in the archive literature (Gulec et al., 2004, 2005; Jeon et al., 2008; Rowe and Abdelaal 2016; Abdelaal and Rowe 2017, 2023; Abdelaal et al., 2023; E Silva et al., 2021; 2022, 2023). Abdelaal and Rowe (2017) immersed a HDPE GMB in three high pH synthetic solutions at five different temperatures and reported antioxidant depletion results (Stage I) after a 3-year immersion period. The immersion solutions had pHs of 9.5, 11.5 and 13.5, and metal concentrations that simulated those found in gold and silver PLS (excluding the cyanide for safety reasons). It was shown that antioxidants detected by the standard oxidative induction time test (Std-OIT) fully depleted at 95, 85 and 75 °C, reaching a residual value of approximately 3 min. The most rapid reductions occurred at pH 13.5, followed by pH 11.5 and 9.5 and at greater rates at higher temperatures. For antioxidants detected by the high-pressure OIT test (HP-OIT), increasing the pH from 9.5 to 13.5 greatly increased both the antioxidant depletion rates and the residual HP-OIT_r values. For instance, at 85 °C, there was a very fast depletion in pH 13.5 but only to HP-OIT_r ≥ 0.9 HP-OIT₀ (i.e., 90% of the initial HP-OIT value, HP-OIT₀). In pH 11.5 and 9.5, the HP-OIT depletion was slower compared to pH 13.5 but to lower residual values of 0.67 HP-OIT₀ at pH 13.5, and 0.25 HP-OIT₀ at pH 9.5. Thus, pH 13.5 was the most aggressive solution for the antioxidant depletion of the GMB (based on both Std- and HP-OIT tests), followed by pH 11.5 and 9.5.

The degradation in physical and mechanical properties of the same GMB in the high pH solutions was reported by Abdelaal and Rowe (2023). There was a decrease in HLMI values due to degradation in all three solutions at 95 °C and 85 °C, suggesting that cross-linking was the dominant degradation mechanism. The rate of degradation was fastest at pH 13.5, followed by 11.5 and 9.5. Tensile break strength also showed degradation at these two temperatures following the same pH dependency. However, nominal failure to 50% of the initial value was only reached at 95 °C in the pH 13.5 solution. For the variation in SCR at 85 °C, there was an early reduction to about 58, 54 and 45% of the initial value (i.e., SCR_m) after 7.5, 6 and 2 months of incubation at pH 9.5, 11.5 and 13.5, respectively. After being retained at these values for the subsequent two years, SCR further decreased to reach 21, 19 and 9% of the initial SCR value at pH 9.5, 11.5 and 13.5, respectively, by the end of

three years.

An investigation of the same GMB in pH 13.5 for a period of up to 6.3 years was then reported by Abdelaal et al. (2023) but only at 85 °C. The primary differences from the findings presented by Abdelaal and Rowe (2023) were the reaching of nominal failure based on tensile break strength at 4.3 years and a continued reduction in HLMI to about 30% of its initial value. While these studies provided the estimates of the GMB degradation stages in alkaline PLS at elevated temperatures, the incubation duration reported (even up to 6.3 years) was not sufficient to establish the degradation rates at temperatures below 85 °C required to predict the time to nominal failure (t_{NF}) of the GMB at specific field temperatures.

The current study provides an additional 6.3 years of ageing data after Abdelaal and Rowe (2017, 2023), presenting a total of 9.3 years of data in the three high pH solutions at different temperatures. The objectives of this paper are to (a) improve Stage I predictions reported by Abdelaal and Rowe (2017) by providing updated depletion rates at 65 and 40 °C; (b) examine the degradation in HLMI, tensile, and SCR at different temperatures and establish the durations of Stages II and III using Arrhenius modelling at field-specific temperatures; and (c) provide the time to nominal failure of the GMB in high pH solutions under field conditions.

2. Experimental investigation

2.1. Oven ageing and immersion solutions

Double-sided immersion tests (ASTM D5322, 2023) were used to examine the change in the GMB properties with ageing. This method involves placing 200 × 95 mm coupons in 4 L glass containers filled with synthetic chemical solutions that replicate the effluents in field conditions. The glass containers were incubated in forced air ovens at various temperatures (95, 85, 75, 65 and 40 °C in the current study) to accelerate GMB ageing, with coupons separated by glass rods to ensure that the chemical solution is in full contact with the GMBs. Samples were then periodically extracted at different incubation durations to assess changes in GMB properties over time.

The three synthetic gold/silver PLS solutions investigated by Abdelaal and Rowe (2017, 2023) (Solutions 6–8; Table 1) were used. The solutions were titrated with a 15-mol NaOH solution to achieve the target pH values of 9.5, 11.5 and 13.5. The immersion fluids were replaced every 3 months to prevent the accumulation of depleted antioxidants in the solution and to ensure a consistent pH throughout the entire incubation period.

2.2. Geomembrane examined

The GMB used in this study (Table 2), generically denoted as MxCl5, was the same 1.5 mm black smooth HDPE GMB with hindered amine light stabilizers (HALS) examined by Abdelaal and Rowe (2017, 2023) and Abdelaal et al. (2023). The GMB was manufactured in 2008 using the blown film process and met all the minimum requirements specified by GRI-GM 13 (2021).

2.3. Index testing

Std-OIT (35 kPa/200 °C; ASTM D3895, 20195) and HP-OIT (3500 kPa/150 °C; ASTM D5885, 2020) were conducted in parallel to assess the depletion of antioxidants (Stage I) with different functioning temperature ranges stabilizing the GMB. Degradation of physical and mechanical properties (Stages II and III) was assessed by monitoring: (a) HLMI (21.6 kg/190 °C; ASTM D1238, 2020), primarily used to investigate the onset of measurable degradation and the possible degradation mechanism, i.e., cross-linking or chain scission (b) SCR using the single-point notched constant tensile load test (SP-NCTL at a load equal 30% of the GMB yield stress; ASTM D5397, 2019 Appendix), and (c)

Table 1

Laboratory analyzed composition of different solutions used (mg/L unless noted).

Component ^a	L6 (pH 9.5)	L7 (pH 11.5)	L8 (pH 13.5)
Nominal pH	9.5	11.5	13.5
NaOH titration (ml/L)	0.17	0.4	80
Average pH ^b	9.8 ± 0.3	11.4 ± 0.2	13.4 ± 0.2
Ag ⁺	0.3	0.3	0.3
Al ³⁺	<1.0	<1.0	<1.0
As ³⁺	0.9	0.9	0.9
Ba ²⁺	<0.05	<0.05	<0.05
Cd ²⁺	<0.025	<0.025	<0.025
Ca ²⁺	0.42	0.64	0.86
Co ²⁺	0.03	0.03	0.03
Cu ²⁺	9	9	9
Fe ²⁺	<0.05	<0.05	<0.05
Li ⁺	<0.05	<0.05	<0.05
K ⁺	173	181	198
Mg ²⁺	4	2.8	0.13
Mo ⁶⁺	0.68	0.56	0.74
Mn ²⁺	<0.05	<0.05	<0.05
Na ⁺	60	138	27,500
Ni ²⁺	<0.3	<0.3	<0.3
Pb ²⁺	<0.03	<0.03	<0.03
S ⁶⁺	99.5	91.6	124
Zn ²⁺	0.02	0.02	0.02
Cl ⁻	<0.5	<0.5	<0.5
O ^{2-a}	0.59	0.59	0.59
OH ^{-a}	43	9440	20,410
SO ₄ ²⁻	300	300	300
Surfactant ^c (ml/l)	0	0	0

^a Metal ions were analyzed using inductively coupled plasma-mass spectrometer (ICP-MS), while the anions were analyzed using Ion chromatography (IC).

^b Average pH (average of 18 values) measured at the times of incubation solution replacement every 1.5 months during the first 3 years of incubation (Abdelaal and Rowe 2017).

tensile break strength and elongation (Type V; ASTM D6693, 2020). Tensile specimens taken from both the machine direction (MD) and cross-machine direction (XD) of the GMB were tested. However, since the results were similar, only the XD values are reported herein. The SCR specimens were taken in the cross-machine direction, as per ASTM D6693, 2020.

3. Results and discussion

3.1. Effect of pH and temperature on geomembrane properties

3.1.1. Antioxidant depletion

For the three solutions examined, Std-OIT exhibited a rapid early-time depletion followed by a notably slower later-time depletion (Fig. 1). Thus, depletion patterns were described using a double exponential decay function at two different rates, i.e., a four-parameter model (Abdelaal and Rowe 2014b) given by:

$$\text{OIT}_t / \text{OIT}_0 = ae^{-s_1 t} + be^{-s_2 t} \quad (1)$$

where t refers to the incubation time (months); $\text{OIT}_t / \text{OIT}_0$ is the normalized Std-OIT value at any time t after ageing (unitless); s_1 is the early-time depletion rate (month^{-1}); s_2 is the later-time depletion rate (month^{-1}); and a and b are constants determining the initial amplitudes of the decay function, such that $a + b = 1.0$.

The additional 6.3 years beyond the time reported by Abdelaal and Rowe (2017) resulted in complete depletion at 65 °C and improved estimates of both the early- and later-time depletion rates at 40 °C. At 65 °C, the later-time depletion rates at pH 9.5 and 11.5 were only slightly slower compared to Abdelaal and Rowe (2017), while the rate at pH 13.5 exhibited no change (Table 3). Based on these rates, the calculated time to reach Std-OIT_r of 3 min at 65 °C was 64, 54 and 38

Table 2

Geomembrane properties.

Properties	Method	Unit	Mean ± SD
Nominal thickness	ASTM D5199	mm	1.5
GMB designator	–	–	MxC15
Manufacturing date	–	–	May 2008
GMB Density	ASTM D1505	g/cc	0.946
Standard oxidative induction time (Std-OIT; 200 °C/35 kPa)	ASTM D3895, 2019	min	160 ± 1.5 ^a
High-pressure oxidative induction Time (HP-OIT; 150 °C/3500 kPa)	ASTM D5885, 2020	min	960 ± 17
Suspected HALS ^b	–	–	Yes
Crystallinity	ASTM D3418	%	50.5 ± 0.7
HLMI (21.6 kg/190 °C) ^c	ASTM D1238	g/10min	12.9 ± 0.4
LLMI (2.16 kg/190 °C) ^d	–	–	0.115 ± 0.001
HLMI/LLMI ratio	–	–	111
Single point stress-crack resistance (NCTL-SCR)	ASTM D5397, 2019	hours	800 ± 90
Tensile properties (<i>machine direction</i>)			
Strength at yield	ASTM D6693, 2020	kN/m	27.8 ± 1.2
Strength at break	Type (IV)	kN/m	49.8 ± 2.7
Strain at yield	–	%	20.6 ± 0.7
Strain at break	–	%	818 ± 18
Tensile properties (<i>cross-machine direction</i>)			
Strength at yield	ASTM D6693, 2020	kN/m	29.1 ± 1.0
Strength at break	Type (IV)	kN/m	50.7 ± 2.7
Strain at yield	–	%	18.3 ± 0.7
Strain at break	–	%	857 ± 23

^a GMB initial properties are subjected to small changes with time due to storage of the roll in room temperature for long period, variability of the material within the same roll (e.g., distribution of additives; resin imperfections), and periodic calibration of the testing equipment.

^b Trace nitrogen analysis was conducted and reported by Ewais et al. (2014) inferring the presence of HALS.

^c High load Melt Index.

^d Low load Melt Index.

months for the pH 9.5, 11.5 and 13.5 solutions, respectively. The Std-OIT data at 40 °C displayed a shallower curvature than initially projected over the first three years, leading to faster early-time depletion rates, but slower later-time rates than those reported in Abdelaal and Rowe (2017) (Fig. 1; Table 3). Updated rates supported the conclusions of Abdelaal and Rowe (2017) that increasing the pH from 9.5 to 13.5 decreased the early-time Std-OIT depletion rates but increased the later-time depletion rates. This was attributed to the different effects of alkaline media on the phosphite antioxidants captured by the early-time depletion rates and the hindered phenols depletion predominantly captured by the later-time depletion rates (Abdelaal and Rowe 2017). Despite such change in pH effect on the different depletion rates, the later-time depletion rates governed the time to depletion to the residual values where pH 13.5 had the fastest time to depletion at different temperatures, followed by pH 11.5 and then pH 9.5 (Table 3). The change in the effect of pH on the early- and later-time depletion rates may affect the predictions of the antioxidant depletion stage depending on the duration of experimental data used to establish the depletion rates. Further discussion of this point is presented in Section 3.2.2.

For the antioxidants detected by the HP-OIT test, there was a depletion to very high residual values (see Fig. S1 in Supplementary Material), a trend often observed in HDPE GMBs with suspected high molecular weight HALS (Ewais et al., 2014; Rowe and Abdelaal 2016; Abdelaal et al., 2019; Zafari et al., 2023a). Thus, depletion was modelled using a first-order exponential decay function with a residual value, viz:

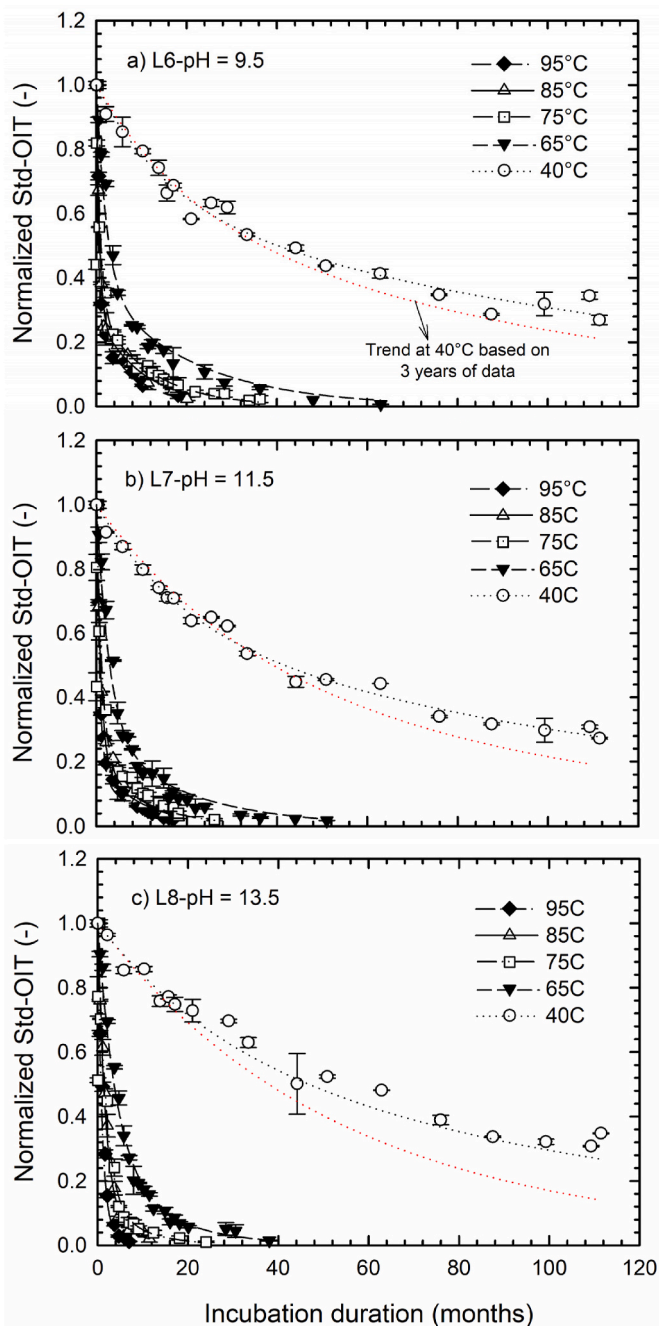


Fig. 1. Variation with incubation time of normalized Std-OIT (OIT_t/OIT_0) in (a) L6-pH = 9.5; (b) L7-pH = 11.5; and (c) L8-pH = 13.5. Red dotted line represents the depletion trend reported by Abdelaal and Rowe (2017) based on 3-years of data. Vertical bars represent the range of values.

$$OIT_t / OIT_0 = ae^{-st} + OIT_r / OIT_0 \quad (2)$$

where s is the single antioxidant depletion rate; OIT_r/OIT_0 is the normalized residual OIT value; and a in this case equals $(1 - OIT_r/OIT_0)$.

At 85 °C (Fig. 2) and all other temperatures (Table S1), the HP-OIT_r and depletion rates at pH 13.5 obtained based on the 9.3-year data were similar to the values obtained from Abdelaal and Rowe (2017) and Abdelaal et al. (2023). However, at pH 9.5 and 11.5, longer incubation revealed that the HP-OIT residual values were different from the values estimated based on the 3-year study and stabilized at approximately 23% of HP-OIT₀ at pH 9.5, while at pH 11.5 it is estimated to reach 30% of HP-OIT₀ based on the best fit of current data. Despite these changes in

Table 3

Std-OIT depletion rates (s_1 and s_2) estimated at the five laboratory incubation temperatures.

Temp. (°C)	Solution pH	Early-time rate, s_1		Later-time rate, s_2		Time to Std-OIT _r (months) ^b
		Current 9.3-year study	3-year study ^a	Current 9.3-year study	3-year study ^a	
95	9.5	2.4	2.4	0.12	0.12	21
	11.5	1.4	1.4	0.13	0.13	17
	13.5	1.1	1.1	0.22	0.22	6
85	9.5	1.45	1.45	0.098	0.098	27
	11.5	1.03	1.03	0.10	0.10	23
	13.5	0.6	0.6	0.15	0.15	12
75	9.5	1.1	1.1	0.085	0.085	34
	11.5	0.79	0.79	0.09	0.09	28
	13.5	0.55	0.55	0.12	0.12	18
65	9.5	0.45	0.45	0.047	0.055	64
	11.5	0.35	0.35	0.050	0.065	54
	13.5	0.25	0.25	0.070	0.070	38
40	9.5	0.06	0.05	0.007	0.010	NR
	11.5	0.05	0.03	0.007	0.010	NR
	13.5	0.04	0.02	0.008	0.014	NR

Note: NR = not reached after 9.3 years.

^a Abdelaal and Rowe (2017).

^b Length of Stage I calculated using the 4-parameter exponential equation and a residual Std-OIT ($Std-OIT_r$) = 3min or 0.02 Std-OIT₀ for every solution.

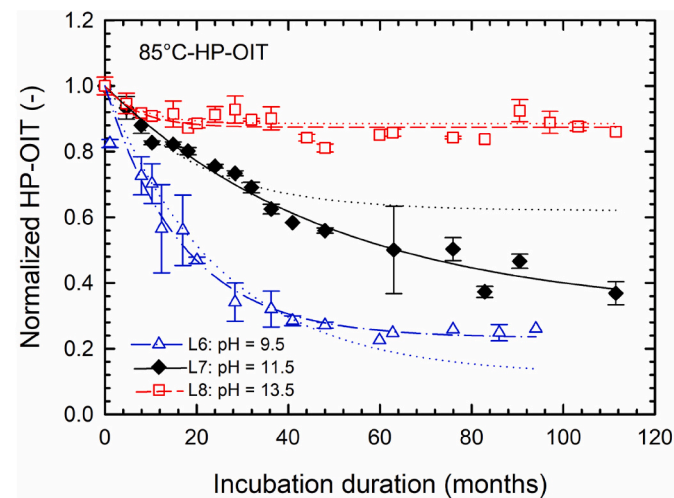


Fig. 2. Variation with incubation time of normalized HP-OIT at 85 °C for the three different high pH solutions. Dotted lines represent the depletion trends reported by Abdelaal and Rowe (2017) based on 3-years of data.

the residual values at pH 9.5 and 11.5, the behaviour was still consistent with the 3-year study since increasing the pH from 9.5 to 13.5 increased the residual value. This implies that increasing the pH retarded the depletion of the HALS which is typically reflected in the HP-OIT residual values (Abdelaal and Rowe 2017). In terms of the depletion rates, Abdelaal and Rowe (2017) reported that HP-OIT depletion rates were consistent with later-time Std-OIT depletion rates during the initial three years in which there was an increase in rates as pH increased from 9.5 to 13.5. However, the current data revealed that the HP-OIT depletion rates (s) at pH 9.5 were higher than at pH 11.5 but were still lower than at pH 13.5 at all temperatures. This inconsistency in the effect of pH on HP-OIT and later-time Std-OIT depletion rates may be attributed to the different effects of pH on the different antioxidants detected by the two tests. Specifically, increasing the pH from 9.5 to 13.5 is expected to reduce the depletion of the HALS (as inferred from the HP-OIT residual values) detected solely by the HP-OIT and increase the hindered phenol depletion detected by both tests (Scheirs 2009; Abdelaal and Rowe 2017). Consequently, the HP-OIT depletion rate is likely influenced by

the pH effects on both antioxidants. This emphasizes the need for extended immersion tests to accurately assess residual HP-OIT values, and suggests that while depletion rates established over three years may provide a conservative assessment of Stage I depletion, they may not fully reflect long-term behaviour.

3.1.2. High load melt index (HLMI)

The present study extends the findings from Abdelaal and Rowe (2023) and Abdelaal et al. (2023) to cover periods of up to 4.2 years at 95 °C (Fig. 3a), 7.5 years at 85 °C (Fig. 3b) and 9.3 years at 75 °C (Fig. 3c). Results collected at 95 °C and 85 °C suggest consistent cross-linking reactions in all three solutions, leading to an increase in the polymer's molecular weight and consequently to a decrease in the melt

index value (Hsuan and Koerner 1998; Scheirs 2009; Grause et al., 2020). At 95 °C, HLMI values reached a minimum of 10% HLMI₀ after 28, 36 and 51 months of incubation in pH 13.5, 11.5 and 9.5, respectively. In addition, the time to the onset of measurable degradation decreased with increasing pH. Similar trends were observed at 85 °C with normalized values reaching less than 20% HLMI₀ after 90 months, although in this case, the decrease occurred at a slower rate compared to 95 °C and with a less significant pH dependency.

At 75 °C, HLMI results in pH 9.5 and 11.5 were retained at the initial value for 63 months before displaying a consistent increase to about 120% and 110% of HLMI₀, respectively. The HLMI value then remained constant at pH 9.5, while at pH 11.5 it further decreased to reach the HLMI₀ value at the end of incubation. At pH 13.5, there was retention at HLMI₀ for 88 months followed by a 15% decrease over the subsequent 6 months and then an increase back to the initial value. This suggests that at 75 °C chain scission and cross-linking reactions were both taking place simultaneously and counteracted each other (Abdelaal and Rowe 2014a; Abdelaal et al., 2015, 2019, 2023), after 63 months of incubation.

The HLMI data suggest that there might be a critical temperature threshold between 85 and 75 °C where the kinetics of cross-linking/chain-scission reactions change (Celina et al., 1998; Likozar and Krajnc 2011; Abdelaal et al., 2015). Below this temperature, the relative rates of these mechanisms could be similar, therefore masking GMB degradation. The chemical solutions also have the potential to affect the balance between these reactions (McDonnell et al., 2017), altering their relative rates and leading to divergent patterns such as those depicted in Fig. 3c. For this reason, HLMI results were not used to estimate the duration of Stages II and III and, thus, t_{NF} of the GMB in this study. Rather, the assessment of degradation stages was based on tensile and SCR properties, discussed in the next sections.

3.1.3. Tensile properties

Among the various tensile properties, only break strength and percent elongation were used to assess GMB degradation. This is due to their consistent decrease in values irrespective of degradation mechanisms, in contrast to the behaviour observed with HLMI. Yield properties were not relied upon because they generally show insignificant changes due to ageing (Schrauwen et al., 2004; Rowe et al., 2010; Ewais and Rowe 2014; Rowe and Shoaib 2017).

Break strength (F_B) and percent elongation at break (ϵ_B) in the cross-machine direction of the GMB decreased to reach nominal failure in all three solutions at 95, 85, and 75 °C (Fig. 4). Both properties showed a scatter around the initial values before they significantly decreased, introducing some uncertainties in defining the onset of measurable degradation and, thus, the length of Stages II and III. Nevertheless, F_B and ϵ_B were estimated to reach nominal failure between 30 and 45 months of incubation at 95 °C (the lower bound indicating the behaviour in pH 13.5) (Fig. 4a and b); between 47 and 60 months at 85 °C (Fig. 4c and d); and between 80 and 96 months at 75 °C (Fig. 4e and f). Although the differences between the estimated t_{NF} values based on break strength and break elongation were small at a given pH and temperature, the values were slightly greater for break elongation. After 9.3 years from the onset of incubation, there was no degradation in tensile properties at and below 65 °C (Fig. S2).

3.1.4. Stress-crack resistance

SCR data are presented for durations of up to 83 months at 85 °C and 75 °C, and 112 months at 65 °C and 40 °C (Fig. 5). Results at 95 °C are included in the Supplementary Material (Fig. S3).

The additional data at 85 °C resulted in the SCR specimens failing in less than 3 h (<1% SCR₀) for all three solutions (Fig. 5a). At 75 °C, SCR decreased to SCR_m values of 34, 35, and 27% of SCR₀ at pH 9.5, 11.5, and 13.5, respectively. After 36 months of incubation, SCR further decreased to reach less than 5% of SCR₀ by the end of 83 months (Fig. 5b). At 65 °C, SCR stabilized at values between 28 and 32% of SCR₀,

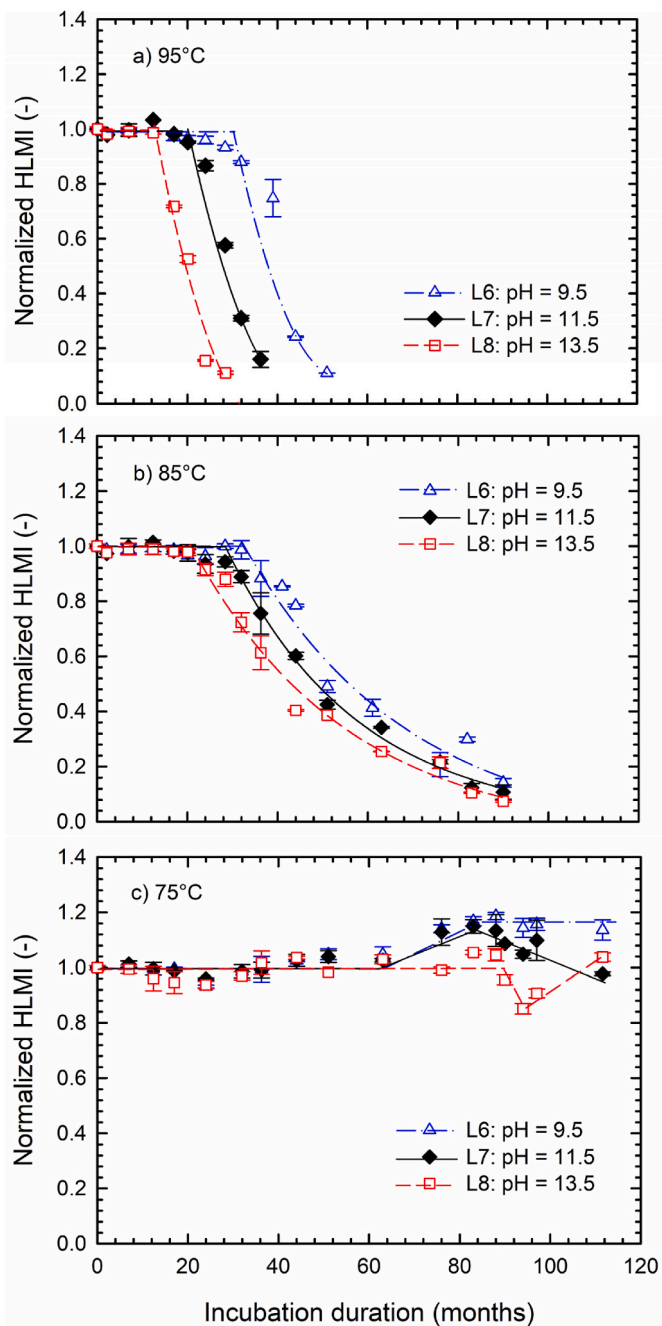


Fig. 3. Variation with incubation time of normalized high-load melt index at (a) 95 °C; (b) 85 °C; and (c) 75 °C. Vertical bars represent the range of measured values.

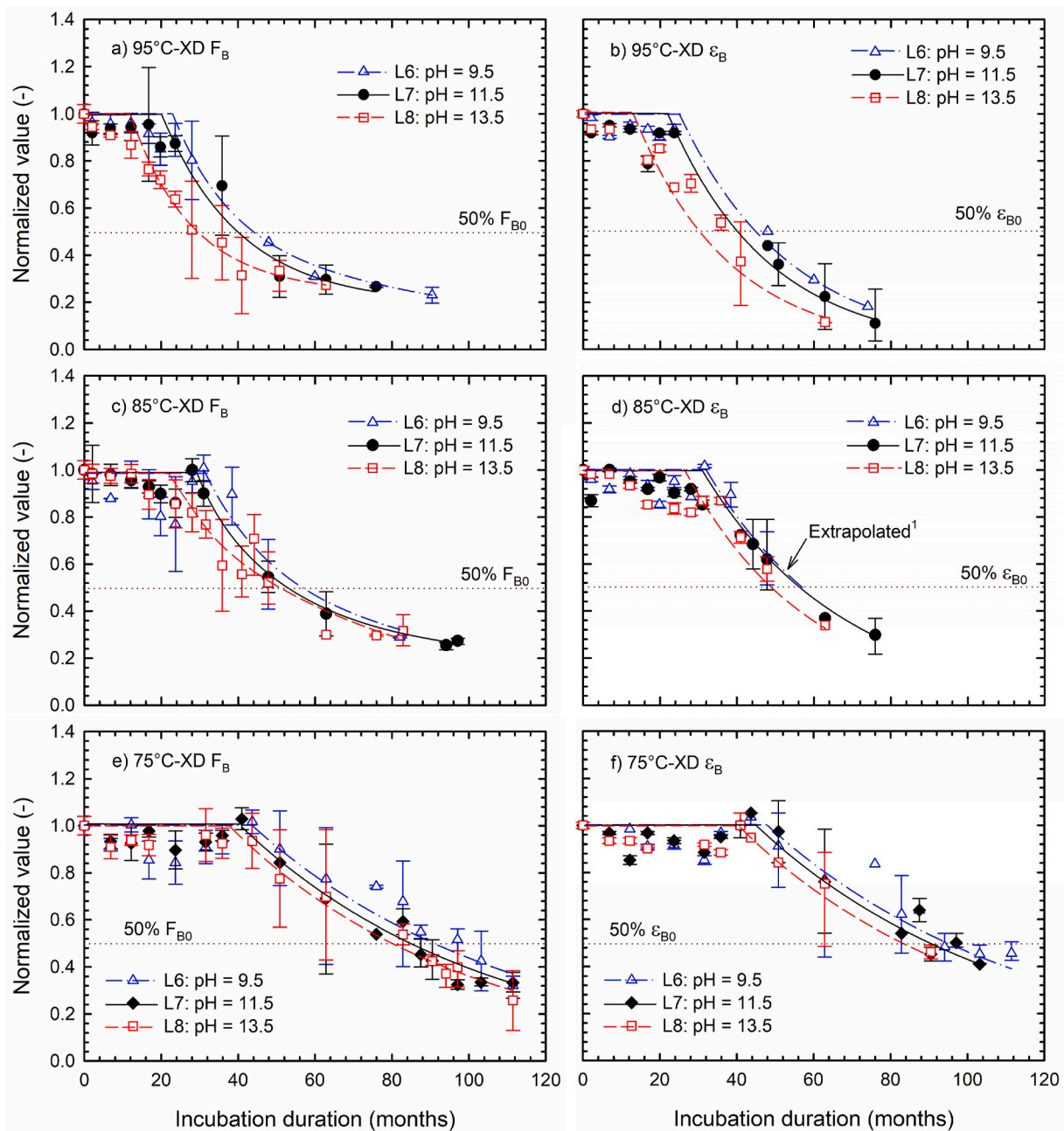


Fig. 4. Variation with incubation time of cross-direction break strength (a, c, e) and elongation (b, d, f) at 95 °C, 85 °C and 75 °C. Vertical bars represent the range of measured values. ¹Results beyond 48 months at pH 9.5 encountered limitations; thus, an attempt was made to find the best possible fit for the data available up to 48 months.

in all three solutions until the end of the incubation period examined (Fig. 5c). At 65 °C, the SCR_m values were the lowest, since at 40 °C the values increased to 49–66% of SCR_0 (Fig. 5c). This agrees with [Ewais and Rowe \(2014\)](#), who found a decrease in SCR_m as the immersion temperatures decreased from 95 to 55 °C, owing to the dominance of the annealing effect (which enhances SCR; [Lu et al., 1992](#)) over chain disentanglement (which decreases SCR; [Brown et al., 1991](#)) at higher temperatures. The difference between the mean values of the normalized SCR_m for the three high pH solutions was statistically significant (ANOVA one-way analysis; 95% confidence level) at 85 °C. Nevertheless, the ANOVA test showed no statistically significant difference between the mean values of SCR_m at 75, 65 and 40 °C. Although it is possible that the pH affected the SCR_m at 85 °C, the difference could also be attributed to the random variability of samples (e.g., crystallinity or

the magnitude of residual stresses across the GMB roll; [Rowe et al., 2019](#)).

At 85 °C, t_{NF} based on SCR was around 35, 34 and 31 months at pH 9.5, 11.5 and 13.5, respectively, as shown by [Abdelaal and Rowe \(2023\)](#). At 75 °C, t_{NF} was about 58, 57 and 56 months at pH 9.5, 11.5 and 13.5, respectively. Thus, temperature had a greater effect on the t_{NF} compared to pH. The results at 95 °C were significantly affected by morphological changes in the polymer due to annealing ([Abdelaal et al., 2015](#)), leading to a slower degradation rate compared to 85 °C. For instance, at 95 °C, after SCR stabilized at approximately 100, 78 and 75% of SCR_0 , it further decreased to reach nominal failure at 80, 56 and 52 months of incubation at pH 9.5, 11.5 and 13.5, respectively (Fig. S3). Therefore, the SCR degradation results at 95 °C could not be used as part of the Arrhenius relationship involving the data at and below 85 °C.

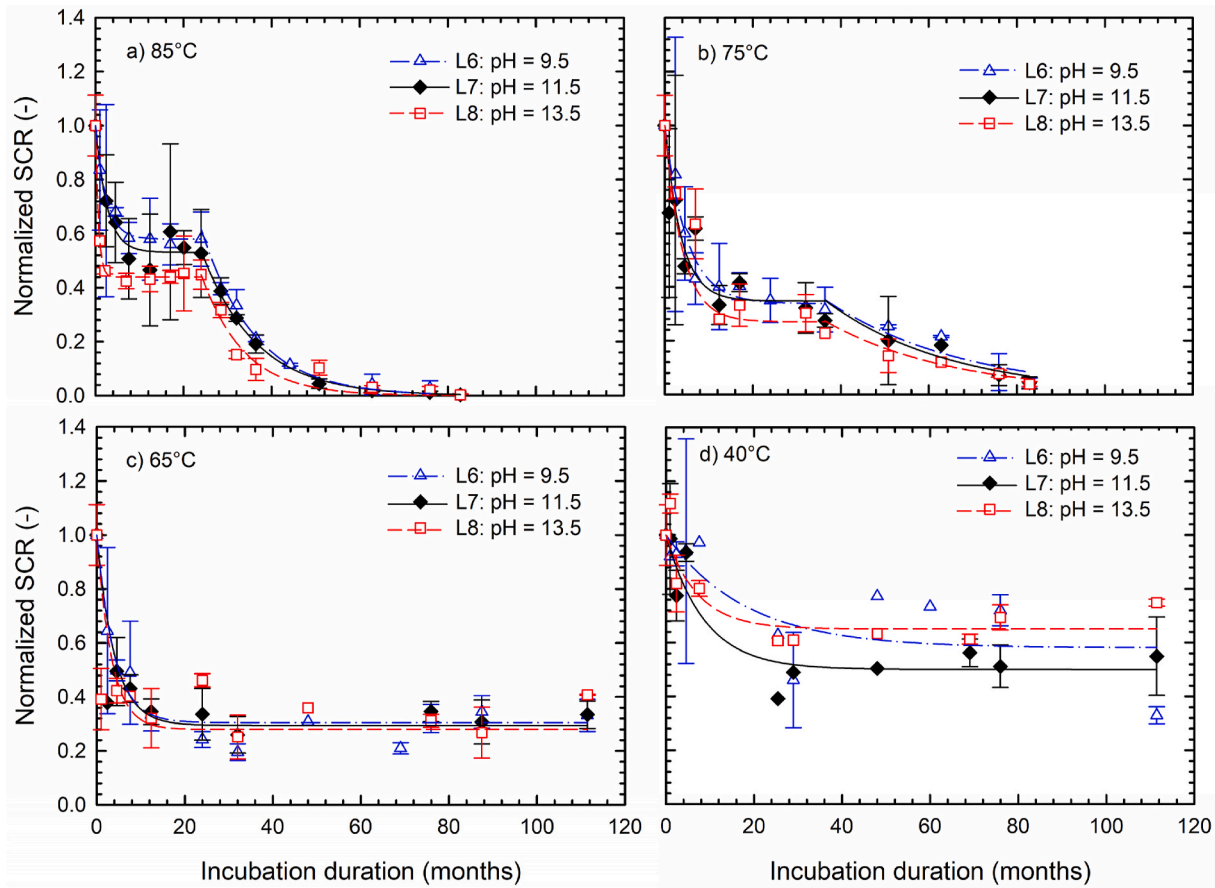


Fig. 5. Variation with incubation time of SCR at (a) 85 °C, (b) 75 °C, (c) 65 °C and (d) 40 °C. Vertical bars represent the range of measured values.

3.1.5. Discussion of the GMB degradation in high pH solutions at elevated temperatures

The duration of Stages I, II and III based on cross-machine break strength/elongation and SCR, are provided at 95, 85 and 75 °C in Table 4. Due to the inconsistent pH dependency observed in HP-OIT depletion, and the more conservative results obtained from Std-OIT (i.e., full depletion between 95 and 65 °C in all three solutions), the Std-OIT test will be solely used to characterize Stage I of the three stage conceptual degradation model. The duration of Stage III was obtained by subtracting t_{NF} (i.e., time to reach 50% of F_{B0} and ϵ_{B0} ; or 50% SCR_m) from the estimated onset of measurable degradation, marked by the endpoint of horizontal lines in Fig. 4, and the endpoint of plateau regions

in Fig. 5. The duration of Stage II was then calculated by subtracting the durations of Stages I and III from t_{NF} . Plots depicting the variation of different index properties at 75 °C at pH 9.5, 11.5 and 13.5 are provided in the Supplementary Material (Fig. S4).

The data collected over 9.3 years at 95, 85, and 75 °C indicate that the duration of Stage III and t_{NF} based on tensile break properties and SCR correlates well with Stage I durations based on Std-OIT in the three solutions: both Stage III and t_{NF} decreased as the pH of the immersion solution increased. This is consistent with the degradation trends observed in SCR and machine-direction break strength at 95 °C and 85 °C over the first three years investigated by Abdelaal and Rowe (2023). Furthermore, SCR at 85 °C and 75 °C degraded much earlier

Table 4
Comparison of GMB degradation stages and time to nominal failure for the three high pH solutions.

Index Property	Units	95 °C			85 °C			75 °C			
		L6	L7	L8	L6	L7	L8	L6	L7	L8	
Length of Stage I	Std-OIT*	month	21	17	6	24	23	12	34	28	18
Length of Stage II	XD- F_B	month	2	3	6	4	6	8	10	13	20
	XD- ϵ_B		4	5	7	7	8	14	14	17	23
	SCR	NU				^b	1	12	2	8	18
Length of Stage III	XD- F_B	month	22	20	18	27	24	32	47	45	42
	XD- ϵ_B		20	18	17	26	25	23	48	46	42
	SCR	NU				11	10	7	22	21	20
Time to nominal failure	XD- F_B **	month	45	40	30	55	53	52	91	86	80
	XD- ϵ_B **		45	40	30	57	56	49	96	91	83
	SCR ^a	NU				35	34	31	58	57	56

Note: NU = not used in the current investigation; NR = not reached.

* Depletion time to Std-OITr = 3 min.

** Time to nominal failure when defined based on the property reducing to 50% of the initial value.

^a Time to nominal failure when defined based on SCR being reduced to 50% of the stabilized SCR value (SCR_m).

^b No Stage II since the degradation in SCR started before full depletion of Std-OIT.

than tensile break properties (Table 4; Fig. S4), as reported by previous research (Rowe et al., 2009; Ewais et al., 2018; Abdelaal et al., 2023; Zafari et al. 2023b, 2023c). Also, Fig. S4 confirms that the changes observed in HLMI data at 75 °C (particularly after 63 months of incubation) were not just a scatter in the data around the initial values but due to simultaneous chain scission and crosslinking degradation, since break strength and SCR were showing degradation at the same time.

After the depletion of antioxidants detected by Std-OIT to the residual value, the time for the onset of measurable degradation (Stage II) also varied with pH and temperature for both tensile and SCR. However, unlike the behaviour observed in Stages I and III, the length of Stage II was longer at pH 13.5 than 11.5 and 9.5. Abdelaal and Rowe (2023) proposed two hypotheses to explain this atypical pH dependency of Stage II. The first hypothesis suggested a link to the residual antioxidants detected by the HP-OIT test, given that the HP-OIT_r values also consistently increased with increasing pH (Fig. 2; Table S1). If the residual HP-OIT values were not influencing the delay in degradation, the second hypothesis proposed that the immersion solutions interacted differently with the GMB resin, leading to the longer retention of properties at pH 13.5 compared to pH 11.5 and pH 9.5.

The high HP-OIT_r values observed for all three solutions are generally a result of the entrapment of HALS molecules within the GMB thickness, whether by their absorption to carbon black (Müller et al., 2016), or reductions in the polymer free volume (i.e., openings between chains in the amorphous zone; Zeiner and Fischlschweiger 2023). The latter can be further augmented by cross-linking reactions inferred from the HLMI data (Fig. 3), with large molecular size HALS molecules becoming integrated into this narrower, cross-linked network, rendering them immobile (Schlotter and Furlan 1992; Koontz et al., 2010). Regardless of their remaining chemical efficacy, trapped HALS may hinder oxidative attack and degradation reactions through their physical presence, creating a diffusion barrier that can limit the movement of oxygen and other reactive species into the polymer matrix (Roe et al., 1974; Peterlin 1975; Schmidt and Malwitz 2003). This ‘physical hindrance effect’ corroborates the first hypothesis of the duration of Stage II at increasing pH levels.

Determining whether the high residual HP-OIT values or the inherent resistance of the resin itself had a greater impact on increasing Stage II as pH increased from 9.5 to 13.5 would require further experimental investigation. It is possible that the two factors both played a role in explaining the observed Stage II durations in the different pH solutions, with their effects reinforcing or counteracting each other depending on pH conditions.

3.2. Predicting GMB degradation

3.2.1. The Arrhenius relationship

One of the most relevant approaches for extrapolating material performance from thermal ageing to field conditions is the Arrhenius relationship (Laidler 1984; Ancheyta 2017; Kutz 2018). An Arrhenius equation can be expressed as follows:

$$k = Ae^{-\left(\frac{E_a}{RT}\right)} \quad (3)$$

where k is the rate of the reaction or degradation process; A is the pre-exponential factor associated with the frequency of collisions between molecules and with the probability that these collisions result in a reaction (i.e., collision factor); E_a is the activation energy that must be overcome for the reaction to occur (kJ/mol); R is the universal gas constant (8.314 J mol⁻¹ K⁻¹); and T is the temperature in Kelvin.

A log-plot of Equation (3) results in a linear relationship between the reaction rate and the reciprocal absolute temperature, where the slope is $(-E_a/R)$ and the y-intercept is $\ln(A)$. This allows for extrapolations beyond the experimental temperature range, and, when the slope is known, the activation energy can be directly calculated. In this section,

Arrhenius extrapolations of the rates of antioxidant depletion (Stage I) and degradation of mechanical properties (Stages II and III) are used to estimate the duration of degradation stages for the GMB in the different high pH solutions at different temperatures.

3.2.2. Antioxidant depletion based on Std-OIT and HP-OIT

The Arrhenius equation in terms of antioxidant depletion based on OIT can be written as (Hsuan and Koerner 1998):

$$s = Ae^{-\left(\frac{E_a}{RT}\right)} \quad (4)$$

where s could be the early- or later-time antioxidant depletion rate (month⁻¹), if Std-OIT is considered, or the single depletion rate based on HP-OIT (month⁻¹).

The Std-OIT depletion rates derived from the four-parameter model at different incubation temperatures (s_1 and s_2 ; Table 3) were used to establish Arrhenius plots of antioxidant depletion in the three high pH solutions (Fig. 6). Even after many years of ageing, the Arrhenius equations for both early- and later-time depletion rates could still be described by a single E_a (Hsuan and Koerner 1998; Rowe et al. 2008, 2020; Rowe and Ewais 2014; Abdelaal et al., 2019; Zafari et al., 2023b). Due to the observed changes at 40 °C, the energies decreased for s_1 but increased for s_2 relative to Abdelaal and Rowe (2017).

Once the early- and later-time depletion rates were extrapolated using the equations in Fig. 6, the next step involved estimating the values of the exponential fit parameters a and b (unitless) from Equation (1) at the predicted temperatures. The values of the parameter a , estimated from the Std-OIT depletion curves presented in Fig. 1, were

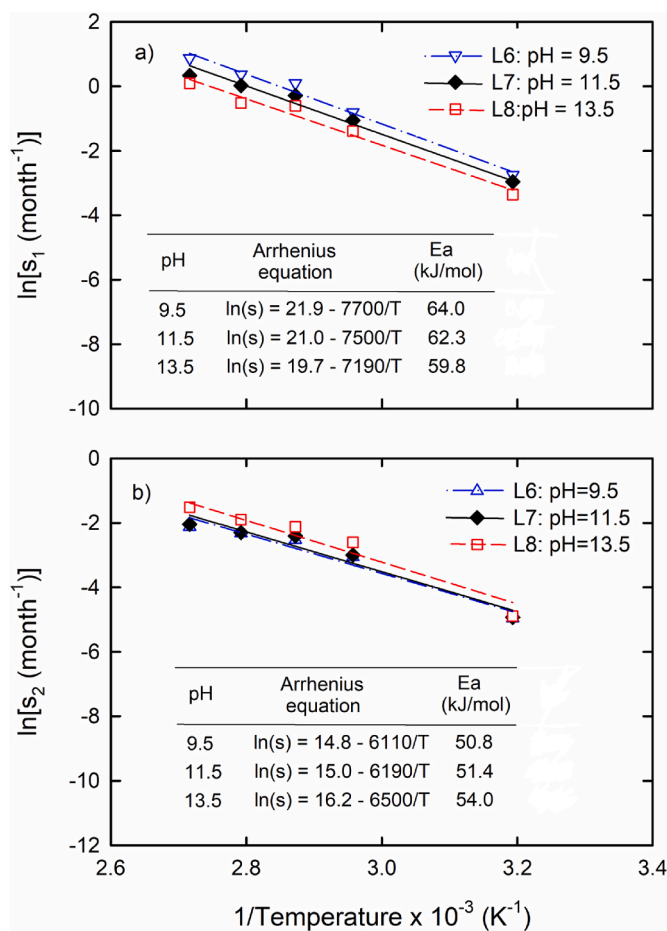


Fig. 6. Arrhenius plots of: (a) early-time and (b) later-time Std-OIT depletion rates from the 4-parameter model.

plotted against the test temperature for each of the high pH solutions. A linear relationship was found, as reported in previous studies (Abdelaal and Rowe, 2014a, 2017). The equations were given by:

$$a_{pH\ 9.5} = 0.007T + 0.13 \tag{5}$$

$$a_{pH\ 11.5} = 0.008T + 0.11 \tag{6}$$

$$a_{pH\ 13.5} = 0.01T + 0.05 \tag{7}$$

where T is the immersion temperature in degrees Celsius.

Parameter b was calculated by subtracting a from the normalized initial Std-OIT value, i.e., ($b = 1.0 - a$). Then, taking 3 min as the residual Std-OIT value ($\sim 2\%$ of Std-OIT₀), Equation (1) was used to calculate the predicted time for depletion (i.e., t_d) for the three high pH solutions at different extrapolated temperatures (Table 5). To account for variability in experimental results and uncertainties linked to predictions, particularly at temperatures significantly lower than the incubation temperatures, a range of Std-OIT depletion rates was predicted for each temperature (Abdelaal and Rowe 2017; Zafari et al., 2023c). These predictions were based on different slopes (activation energies) of the Arrhenius plots depicted in Fig. 6, and included the expected, as well as the maximum and minimum activation energies at a 95% confidence level. The expected activation energy is derived from the best-fit slope of the Arrhenius plot, suggesting a 50% probability that the true activation energy is above or below this value. The minimum value represents the slope above which there is a 95% probability that the true activation energy will fall. Conversely, the maximum value represents the slope below which there is a 95% probability that the true activation energy will fall.

In terms of the early-time depletion rate, the activation energies had a 95% confidence band range of $50 \leq E_a \leq 78$ kJ/mol for pH 9.5, $43 \leq E_a \leq 75$ kJ/mol for pH 11.5, and $42 \leq E_a \leq 77$ kJ/mol for pH 13.5. In terms of the later-time rate, activation energies had a range of $30 \leq E_a \leq 72$ kJ/mol for pH 9.5, $29 \leq E_a \leq 74$ kJ/mol for pH 11.5, and $34 \leq E_a \leq 82$ kJ/mol for pH 13.5. To help illustrate, the slopes for s_1 at pH 9.5 are provided in Fig. S5. The depletion times at high temperatures (95-70 °C) align reasonably well with predictions presented by Abdelaal and Rowe (2017), as the ratio between them is close to unity (Table 6). As

Table 6
Ratio of depletion times (t_d) between current 9.3-year study and the 3-year study by Abdelaal and Rowe (2017).

T (°C)	(Current t_d)/(3-yr study t_d)		
	pH 9.5	pH 11.5	pH 13.5
95	0.9	0.9	1.0
90	0.8	0.9	0.8
85	1.0	1.0	1.0
80	0.9	0.9	0.9
75	1.1	1.1	1.1
70	1.1	1.1	1.1
65	1.2	1.1	1.2
60	1.2	1.3	1.2
55	1.3	1.3	1.2
50	1.2	1.3	1.2
45	1.3	1.3	1.3
40	1.4	1.5	1.4
35	1.5	1.5	1.4
30	1.5	1.6	2.0
25	1.6	1.7	1.5
20	1.6	1.7	1.4
10	1.9	1.8	1.6
5	2.1	2.0	1.4

expected, a significant difference in predictions emerges at lower temperatures given the changes captured at 65 °C and, most importantly, 40 °C.

To further investigate the effect of the incubation duration on Std-OIT depletion predictions, data based on 3 and 12 months of ageing were considered (Table 7). The best-fit (expected) activation energy was used in the Arrhenius plots for each solution. Results show that the 3-month dataset fitted with a two-parameter exponential decay model (i.e., using a single depletion rate) would be misleading, suggesting that the pH 13.5 solution is the least aggressive in terms of antioxidant depletion. This was essentially due to the slower early depletion rates at pH 13.5 than the pH 11.5 and 9.5 solutions. Only after extending the incubation period to at least one year to capture the change in the relative depletion of the different high pH solutions, the Std-OIT predictions were the shortest at pH 13.5, followed by 11.5 and then 9.5. This again was confirmed by the 3-year testing performed by Abdelaal

Table 5
Predicted antioxidant depletion times (years) based on Std-OIT at different extrapolated temperatures.

T (°C)	t_d based on current 9.3-year study ^{a,*}									t_d based on 3-year study ^a		
	pH 9.5			pH 11.5			pH 13.5			pH 9.5	pH 11.5	pH 13.5
	$E_{a_{min}}$	$E_{a_{exp}}$	$E_{a_{max}}$	$E_{a_{min}}$	$E_{a_{exp}}$	$E_{a_{max}}$	$E_{a_{min}}$	$E_{a_{exp}}$	$E_{a_{max}}$	$E_{a_{exp}}$		
95	2.0	1.2	0.8	1.4	0.9	0.4	0.4	0.3	0.2	1.3	1.0	0.3
90	2.5	1.6	1.1	1.9	1.2	0.7	0.6	0.5	0.3	2.0	1.3	0.6
85	3.0	2.2	1.6	2.4	1.8	1.1	1.0	0.9	0.5	2.2	1.8	0.9
80	3.6	2.6	2.4	2.9	2.1	1.7	1.4	1.3	0.7	2.8	2.3	1.4
75	4.3	4.0	3.6	3.7	3.4	2.6	1.8	2.0	1.2	3.7	3.2	1.9
70	5.2	5.2	5.2	4.3	4.5	4.0	2.3	2.9	1.9	4.7	4.0	2.6
65	6.2	7.0	7.9	5.5	6.2	6.0	3.0	4.1	3.0	6.0	5.4	3.5
60	7.6	9.4	12	6.7	8.7	9.4	3.7	5.7	4.9	8.0	6.8	4.9
55	9.0	13	18	8.0	12	14	4.7	8.1	8.0	10	9.0	6.7
50	11	17	28	10	16	23	6.0	11	13	14	12	9.1
45	13	24	43	12	22	36	7.5	16	22	18	17	12
40	16	33	68	15	32	57	10	23	37	24	21	17
35	20	47	110	18	45	92	12	34	64	31	30	24
30	24	66	170	21	63	150	15	49	110	43	39	25
25	30	94	270	27	91	250	19	70	190	57	55	47
20	37	130	500	32	130	430	25	100	340	81	75	72
10	59	290	>1000	52	280	>1000	43	240	>1000	150	160	150
5	75	450	>2000	65	450	>2000	56	360	>2000	210	230	250

Note: Predictions have been rounded to no more than two significant digits.

^{*} t_d = time to Std-OIT depletion assessed based on reaching a residual value of 3 min.

^a Predictions are based on: (i) expected activation energies using the 'best-fit' lines in the Arrhenius plots, indicating a 50% probability that the depletion times are above or below these values; (ii) minimum activation energies, with a 95% probability that the predictions will be greater than these values; and (iii) maximum activation energies, with a 95% probability that the predictions will fall below these values.

Table 7

Expected antioxidant depletion times at different temperatures based on different immersion periods.

Antioxidant depletion times (years)												
T (°C)	9.3-year immersion*			3-year immersion*, ^a			1-year immersion*			3-month immersion**		
	pH 9.5	pH 11.5	pH 13.5	pH 9.5	pH 11.5	pH 13.5	pH 9.5	pH 11.5	pH 13.5	pH 9.5	pH 11.5	pH 13.5
95	1.2	0.9	0.3	1.3	1.0	0.3	1.9	1.2	0.4	0.3	0.3	0.3
90	1.6	1.2	0.5	2.0	1.3	0.6	2.1	1.5	0.7	0.4	0.4	0.5
85	2.2	1.8	0.9	2.2	1.8	0.9	2.5	1.8	1.0	0.5	0.5	0.6
80	2.6	2.1	1.3	2.8	2.3	1.4	2.9	2.2	1.4	0.6	0.7	0.9
75	4.0	3.4	2.0	3.7	3.2	1.9	3.3	2.6	1.8	0.8	0.9	1.2
70	5.2	4.5	2.9	4.7	4.0	2.6	3.9	3.1	2.3	1.1	1.2	1.7
65	7.0	6.2	4.1	6.0	5.4	3.5	4.5	3.7	2.9	1.5	1.6	2.4
60	9.4	8.7	5.7	8.0	6.8	4.9	5.2	4.4	3.6	2.0	2.1	3.4
55	13	12	8.1	10	9.0	6.7	6.0	5.3	4.5	2.7	2.9	4.9
50	17	16	11	14	12	9.1	7.0	6.4	5.7	3.6	3.9	7.2
45	24	22	16	18	17	12	8.2	7.7	7.3	5.0	5.4	11
40	33	32	23	24	21	17	9.8	9.4	9.4	7.1	7.6	16
35	47	45	34	31	30	24	12	12	12	10	11	24
30	66	63	49	43	39	25	15	15	16	14	15	37
25	94	91	70	57	55	47	21	20	22	21	22	58
20	130	130	100	81	75	72	29	27	30	30	33	93

Note: Predictions greater than 10 years have been rounded to no more than two significant digits.

* Length of Stage I calculated using a 4-parameter exponential equation and a residual Std-OIT (Std-OIT_r) = 3min or 0.02 Std-OIT₀ for every solution.

** Length of Stage I calculated using a 2-parameter exponential equation and a residual Std-OIT (Std-OIT_r) = 3min or 0.02 Std-OIT₀ for every solution.

^a Based on [Abdelaal and Rowe \(2017\)](#).

and Rowe (2017) as well as the present study. Extending the incubation period also resulted in longer depletion times, showing that longer term data collection could greatly improve Std-OIT predictions. While the short term Std-OIT data may conservatively capture the long term relative depletion of the same GMB in different solutions or for different GMBs in the same solution, the incubation in the three high pH solutions discussed herein shows that this does not apply for cases in which the relative depletion changes with time. As such, longer incubation is needed until such change in the depletion behaviour is observed to ensure consistent predictions with long term data.

Depletion rates and residual values based on HP-OIT (Table S1) were also used to establish Arrhenius plots for the three solutions (Fig. S6). Table S2 shows the predicted times to depletion based on HP-OIT data and the corresponding HP-OIT_r values. At pH 9.5, the depletion based on current data was sufficient to allow the evaluation of the residual values at any test temperature. This improved the predictions made by [Abdelaal and Rowe \(2017\)](#), who assumed a constant HP-OIT_r of 80 min across all temperatures. Due to significantly slower depletion rates at pH 11.5 compared to pH 9.5 and 13.5, the depletion time (t_d) was consequently longer for that particular solution.

3.2.3. Stages II and III based on tensile properties

The estimated lengths of Stages II and III (i.e., Δt_{II} and Δt_{III}) based on cross-direction break strength and elongation at 95, 85 and 75 °C (Table 4) were used in Arrhenius plots for extrapolating mechanical property changes at lower temperatures. By defining η = 1/Δt_{II} and γ = 1/Δt_{III} as the degradation rates of tensile properties of the GMB during Stages II and III, respectively, Equation (4) can be rewritten as ([Abdelaal et al., 2014b; Ewais et al., 2018](#)):

$$\eta = Ae^{-\left(\frac{E_a}{RT}\right)} \tag{8}$$

and

$$\gamma = Ae^{-\left(\frac{E_a}{RT}\right)} \tag{9}$$

The Arrhenius relationships for η and γ are presented in Figs. 7 and 8, respectively, for the three high pH solutions. Despite the uncertainty in defining when Stage II ended and Stage III began, current tensile data allowed for extrapolations of property changes using single linear

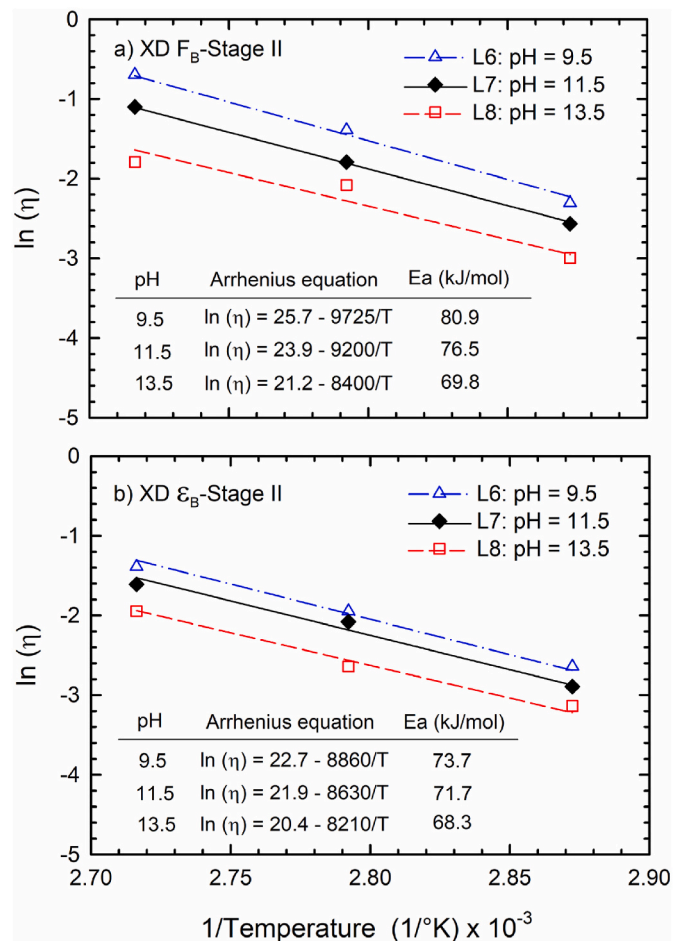


Fig. 7. Arrhenius plots for Stage II based on: (a) cross-machine tensile break strength (F_B) and (b) break elongation (ε_B) for the three high pH solutions.

Arrhenius equations. The estimated Δt_{II} and Δt_{III} from these equations, along with the length of Stage I based on Std-OIT, were compiled to calculate t_{NF} at a range of different temperatures (Tables 8–10). The

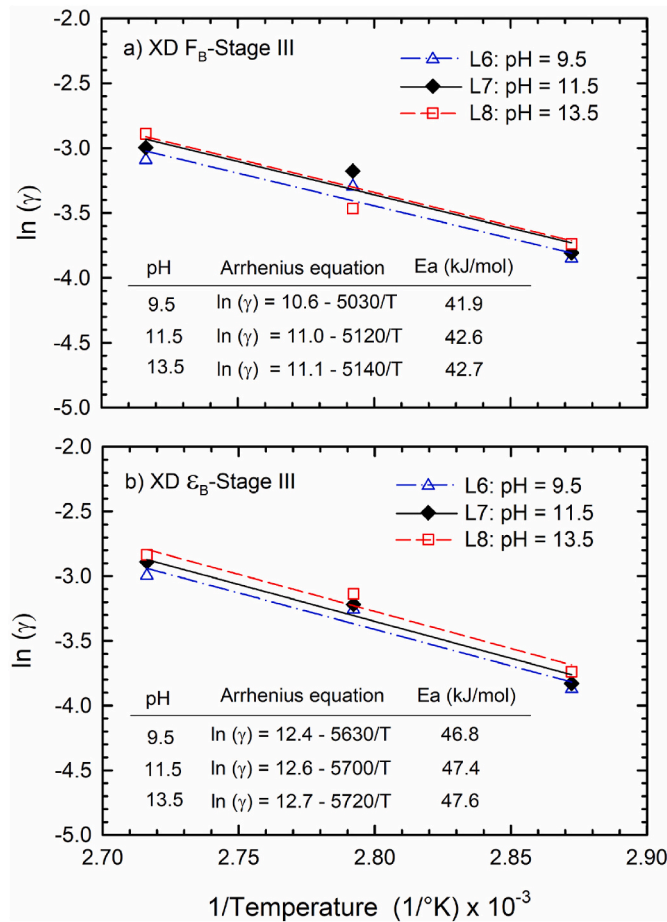


Fig. 8. Arrhenius plots for Stage III based on: (a) cross-machine tensile break strength (F_B) and (b) break elongation (ϵ_B) for the three high pH solutions.

observed t_{NF} values exceeded predictions by up to 22% (e.g., at 95 °C), and were lower by up to 12% at lower temperatures (e.g., 75 °C).

The Arrhenius plots of Stage II degradation rates (Fig. 7) yielded a decreasing E_a and pre-exponential factors A as pH increased. While decreasing E_a values imply lower energy barriers for reactions to occur (Menzinger and Wolfgang 1969; Laidler 1984), the simultaneous

decrease in A suggests that the probability of reactants colliding and forming products is also decreasing (Ancheyta 2017). One could then conjecture that although the degradation beyond the full Std-OIT depletion was easier to initiate at pH 13.5 (due to lower E_a), the rate of degradation once initiated was slower (due to lower A) compared to pH 11.5 and 9.5 (Laidler 1987; Ancheyta 2017). This may have led to the increase in the lengths of Stage II (Tables 8–10) at pH 13.5 than at pH 11.5 and 9.5. For Stage III, both E_a and A exhibited a subtle increase with increasing pH degradation rates (Fig. 8). Thus, there was a marginally higher energy barrier for the degradation reactions to occur as pH increased, and once that barrier was overcome, the degradation propagated at slightly faster rates at higher pHs. This is reflected in the decreasing trend of predicted Stage III durations (Tables 8–10) with increasing pH, although differences were small.

The extended incubation suggests that while the pH 13.5 solution was the most aggressive environment in terms of Std-OIT depletion, it was the least aggressive in initiating degradation in Stage II compared to pH 11.5 and 9.5, as was also observed by Abdelaal and Rowe (2023) after 3 years of incubation. In the context of thermo-oxidative degradation of polyethylene, Stage II involves the formation of hydroperoxide (ROOH) molecules up to a critical level (Hsuan and Koerner 1998; Abdelaal et al., 2015). Meanwhile, Stage III comprises the decomposition of ROOH into more reactive free radicals, which subsequently lead to an accelerated chain reaction and auto-oxidation of the polymer (Al-Malaika 2004; Müller 2010). In this case, it is plausible to argue that at pH 13.5, the rate of ROOH formation was slower than at pH 11.5 and 9.5, with a slightly faster rate of decomposition at pH 13.5.

3.2.4. Time to nominal failure based on current SCR data

Since the SCR data at 95 °C was masked by the annealing effect and the incubation duration was not sufficient to observe Stage III degradation at 65 °C, only the 85 and 75 °C SCR data were used to establish Arrhenius plots beyond Stage I. In addition, no Stage II was observed for pH 9.5 at 85 °C (see Table 4) and hence it was not possible to consistently establish the predictions of the durations of Stages II and III for all three solutions. However, the current SCR data was used to predict the degradation of the GMB by directly plotting the Arrhenius relations of the t_{NF} at 85 and 75 °C. In this case, the Arrhenius equation can be rewritten as:

$$\frac{1}{\Delta t_{NF}} = Ae^{-\left(\frac{E_a}{RT}\right)} \tag{10}$$

Table 8

Expected degradation stages and time to nominal failure (years) based on tensile break strength and elongation in L6 (pH = 9.5) at different temperatures.

T (°C)	Break strength (F_B)					Break Elongation (ϵ_B)				
	Stage I ^a	Stage II	Stage III	Predicted t_{NF}	Observed t_{NF}	Stage I ^a	Stage II	Stage III	Predicted t_{NF}	Observed t_{NF}
95	1.2	0.2	1.7	3.1	3.8	1.2	0.3	1.6	3.1	3.8
90	1.6	0.2	2.1	3.9	–	1.6	0.4	1.9	4.0	–
85	2.2	0.4	2.5	5.1	4.8	2.2	0.6	2.4	5.2	5.0
80	2.6	0.5	3.1	6.2	–	2.6	0.9	3.0	6.5	–
75	4.0	0.8	3.8	8.5	7.6	4.0	1.3	3.8	9.0	8.0
70	5.2	1.2	4.6	11	–	5.2	1.8	4.8	12	–
65	7.0	1.8	5.8	15	–	7.0	2.7	6.1	16	–
60	9.4	2.7	7.2	19	–	9.4	3.9	7.9	21	–
55	13	4.2	9.1	26	–	13	5.9	10	29	–
50	17	6.7	12	35	–	17	9.0	13	39	–
45	24	11	15	49	–	24	14	17	55	–
40	33	17	19	69	–	33	22	23	78	–
35	47	29	25	100	–	47	34	31	110	–
30	66	49	32	150	–	66	55	42	160	–
25	94	83	42	220	–	94	89	57	240	–
20	130	150	60	340	–	130	150	79	360	–
10	290	470	100	860	–	290	430	150	870	–
5	450	870	140	>1000	–	450	760	220	>1000	–

Note: Numbers rounded to no more than two significant digits. Hence, numbers may not add up exactly due to rounding.

^a Estimated from the Arrhenius equations presented in Fig. 6 (i.e., best-fit activation energies).

Table 9

Expected degradation stages and time to nominal failure (years) based on tensile break strength and elongation in L7 (pH = 11.5) at different temperatures.

T (°C)	Break strength (F_B)					Break Elongation (ϵ_B)				
	Stage I ^a	Stage II	Stage III	Predicted t_{NF}	Observed t_{NF}	Stage I ^a	Stage II	Stage III	Predicted t_{NF}	Observed t_{NF}
95	0.9	0.3	1.6	2.7	3.3	0.9	0.4	1.5	2.8	3.3
90	1.2	0.4	1.9	3.4	–	1.2	0.5	1.8	3.6	–
85	1.8	0.5	2.3	4.6	4.4	1.8	0.7	2.3	4.8	4.7
80	2.1	0.7	2.8	5.6	–	2.1	1.0	2.8	6.0	–
75	3.4	1.1	3.5	7.9	7.2	3.4	1.5	3.6	8.5	7.6
70	4.5	1.6	4.3	10	–	4.5	2.1	4.6	11	–
65	6.2	2.3	5.3	14	–	6.2	3.1	5.8	15	–
60	8.7	3.5	6.7	19	–	8.7	4.5	7.5	21	–
55	12	5.3	8.5	26	–	12	7	10	28	–
50	16	8.2	11	35	–	16	10	13	39	–
45	22	13	14	49	–	22	15	17	54	–
40	32	20	18	70	–	32	23	22	78	–
35	45	33	23	100	–	45	37	30	110	–
30	63	54	31	150	–	63	58	41	160	–
25	91	89	41	220	–	91	94	56	240	–
20	130	150	55	340	–	130	150	77	360	–
10	280	460	100	840	–	280	430	150	870	–
5	450	820	140	>1000	–	450	750	220	>1000	–

Note: Numbers rounded to no more than two significant digits. Hence, numbers may not add up exactly due to rounding.

^a Estimated from the Arrhenius equations presented in Fig. 6 (i.e., best-fit activation energies).

Table 10

Expected degradation stages and time to nominal failure (years) based on tensile break strength and elongation in L8 (pH = 13.5) at different temperatures.

T (°C)	Break strength (F_B)					Break Elongation (ϵ_B)				
	Stage I ^a	Stage II	Stage III	Predicted t_{NF}	Observed t_{NF}	Stage I ^a	Stage II	Stage III	Predicted t_{NF}	Observed t_{NF}
95	0.3	0.4	1.4	2.3	2.5	0.3	0.6	1.4	2.2	2.5
90	0.5	0.6	1.8	2.9	–	0.5	0.8	1.7	3.0	–
85	0.9	0.8	2.1	4.0	3.9	0.9	1.1	2.1	4.1	4.1
80	1.3	1.1	2.6	5.2	–	1.3	1.5	2.6	5.4	–
75	2.0	1.6	3.3	7.0	6.7	2.0	2.1	3.3	7.4	6.9
70	2.9	2.3	4.1	9.4	–	2.9	2.9	4.2	10.1	–
65	4.1	3.3	5.1	13	–	4.1	4.2	5.4	14	–
60	5.7	4.7	6.4	17	–	5.7	6.0	7.0	19	–
55	8.1	7.0	8.1	23	–	8.1	8.8	9.1	26	–
50	11	10	10	32	–	11	13	12	36	–
45	16	16	13	45	–	16	19	16	51	–
40	23	24	17	65	–	23	29	21	73	–
35	34	37	23	94	–	34	45	28	110	–
30	49	58	30	140	–	49	69	38	160	–
25	70	92	40	200	–	70	110	52	230	–
20	100	150	50	310	–	100	170	70	350	–
10	240	410	100	750	–	240	470	150	850	–
5	360	700	140	>1000	–	360	790	210	>1000	–

Note: Numbers rounded to no more than two significant digits. Hence, numbers may not add up exactly due to rounding.

^a Estimated from the Arrhenius equations presented in Fig. 6 (i.e., best-fit activation energies).

where Δt_{NF} is the estimated time to nominal failure, in months.

Since t_{NF} values at 85 and 75 °C were not significantly different among the different high pH solutions, a single E_a representing the average E_a among the three high pH solutions was used. The resulting Arrhenius equation is presented in Fig. 9, while t_{NF} extrapolated at various temperatures is presented in Table 11. As previously indicated, SCR at 85 and 75 °C started to degrade much earlier than tensile, resulting in relatively greater degradation rates and, thus, shorter t_{NF} predictions. This shows that of the GMB’s mechanical properties examined herein, SCR was the most sensitive to degradation (Rowe et al., 2014; Ewais et al., 2018; Zafari et al., 2023c).

3.3. Practical implications

The predicted t_{NF} presented herein was established using immersion tests in which the GMB is exposed to the solution from all sides. In reality, except for a single primary GMB in double lined ponds where there is fluid above and in the drainage layer below the GMB near the sump, the GMB in the field is exposed to the solution from the top surface only

and the bottom surface is exposed to the low hydraulic conductivity layer of the composite liner system. As such, the degradation times reported in the current study are considered conservative estimates of the GMB longevity (i.e., shorter than the field estimations). An approach for estimating Stage I (antioxidant depletion time) in a composite liner configuration was proposed by Rowe et al. (2020) in which the depletion times listed in Table 5 can be conservatively multiplied by a factor of 3.4 at a specific temperature. These adjusted times can then be added to the available durations of Stages II and III based on tensile properties to provide a first estimation of the t_{NF} under field conditions considering the three high pH environments (Table 12). Tables S3–S5 show a breakdown of t_{NF} into Stages I, II and III for every solution.

The temperature of a GMB liner in a gold/silver heap leaching operation can vary depending on a number of factors including geographic location, weather conditions, the ore type, the lixiviant chemistry and the heap height, and it is common for the pregnant liquor to be in the range of 30–50 °C (Thiel and Smith 2004; Ghorbani et al., 2016; Manning and Kappes 2016). Considering a heat-generating operation with the buried liner temperature of 30–50 °C, the t_{NF} based

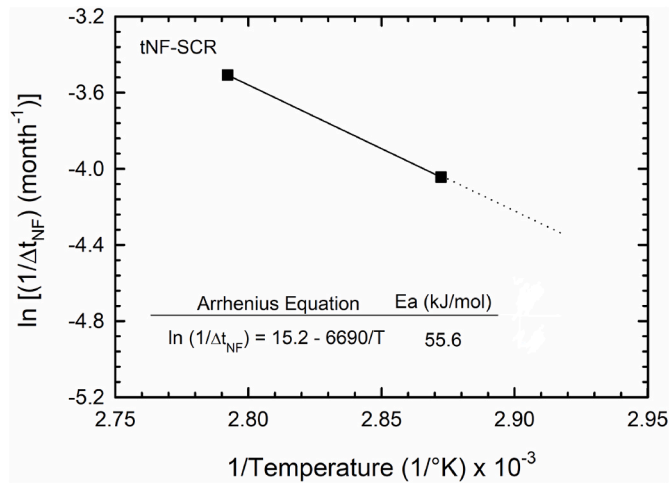


Fig. 9. Arrhenius plot for the time to nominal failure based on SCR for all solutions.

Table 11
Expected time to nominal failure (years) based on SCR at different temperatures immersed in all three solutions (pH 9.5, 11.5 & 13.5).

T (°C)	t_{NF} at 50% SCR_m	Observed
95	1.7	–
90	2.1	–
85	2.8	2.8
80	3.6	–
75	4.8	4.8
70	6.3	–
65	8.4	>9.3
60	11	–
55	15	–
50	21	–
45	29	–
40	41	–
35	58	–
30	82	–
25	120	–
20	180	–
10	390	–
5	600	–

Note: numbers rounded to no more than two significant digits.

Table 12
Expected time to nominal failure (years) based on tensile break strength and elongation for the three high pH solutions in a composite liner configuration.

T (°C)	Break strength (F_B)			Break Elongation (ϵ_B)		
	pH 9.5	pH 11.5	pH 13.5	pH 9.5	pH 11.5	pH 13.5
95	6.0	4.9	3.0	6.0	4.9	3.0
90	7.8	6.3	4.1	7.8	6.4	4.2
85	10	8.9	6.1	11	9.1	6.3
80	12	11	8.4	13	11	8.6
75	18	16	12	19	17	12.2
70	23	21	17	24	22	17.0
65	31	29	23	33	30	24
60	42	40	31	44	42	32
55	58	55	44	60	57	45
50	76	73	60	80	77	62
45	110	100	85	110	110	89
40	150	150	120	160	160	130
35	210	210	180	220	220	190
30	310	300	260	320	310	270
25	450	440	380	470	460	400
20	650	650	580	680	670	600
10	1540	1510	1360	1560	1540	1410
5	>2000	>2000	>2000	>2000	>2000	>2000

on tensile break strength in a composite liner can vary between 310 and 76 years at pH 9.5, 300–73 years at pH 11.5, and 260–60 years for at 13.5 (Table 12). If the liner temperature was consistently at or below 10°C (i. e., for non-heat generating operations), t_{NF} becomes greater than 1000 years for all the high pH solutions examined. An important practical implication that can be drawn from these predictions is that a pH increase in gold/silver PLS from 9.5 to 11.5 may not impact the longevity of the GMB liner as much as an increase to above 13 (particularly through a high dosage of NaOH). However, and irrespective of the pH of the solution, the t_{NF} (estimated considering only the chemical durability component of the GMB service life) can meet the typical design life of a heap leaching operation of 20 years if the liner temperature is maintained below 65°C.

The extrapolations presented here are estimated based on the GMB’s degradation properties under stress-free conditions. Therefore, these estimates assume that the liner design will maintain strains below approximately 3% (Seeger and Müller 2003; Rowe et al., 2019), and certainly less than 5% (Abdelaal et al., 2014a), based on current knowledge.

4. Conclusions

The degradation of a HDPE GMB (Std-OIT₀ = 160 min; HP-OIT₀ = 960 min; SCR₀ = 800 h) in synthetic pregnant liquor solutions from gold and silver heap leaching was assessed using immersion tests at different temperatures. Three solutions (L6-pH 9.5, L7-pH 11.5 and L8-pH 13.5) with essentially the same concentration of metals were considered. The first results of this investigation were reported by Abdelaal and Rowe (2017), who provided predictions for Stage I after monitoring the depletion of antioxidants for three years. Abdelaal and Rowe (2023) and Abdelaal et al. (2023) reported results of high-load melt index (HLMI), stress-crack resistance (SCR) and tensile properties, but further testing was required to predict nominal failure at field temperatures. The present study provides an additional 6.3 years of ageing data to improve Stage I estimates since Abdelaal and Rowe (2017) and to examine the degradation in Stages II and III at 95, 85 and 75 °C, allowing establishing the time to nominal failure (t_{NF}) predictions using Arrhenius modelling. For the specific GMB tested and the exposure conditions examined, the following conclusions can be drawn:

- The assessment of Stage I based on Std-OIT was shown to be more consistent with subsequent GMB degradation than the HP-OIT. At 85 °C, for instance, there was a 90% and 23% residual HP-OIT detected at pH 13.5 and 9.5, respectively, while the HP-OIT was still depleting at pH 11.5, despite the initiation of degradation in the physical and mechanical properties.
- Complete Std-OIT depletion (i.e., depletion to a residual Std-OIT value of 3 min) was achieved at 65 °C for all three solutions, with no significant changes in depletion rates since Abdelaal and Rowe (2017). At 40 °C, the early-time depletion rates only slightly increased, whereas the later-time rates decreased. As such, the predicted times to depletion aligned well with Abdelaal and Rowe (2017) for high temperatures (>70 °C). At lower temperatures, predictions increased by up to 110% due to the changes captured with the additional ageing time. Improved estimates maintained the pH dependency previously reported in which Stage I significantly reduced with increasing pH.
- The length of incubation period affected the rates used to extrapolate Std-OIT depletion. Based on a 3-month dataset, for instance, the pH 13.5 solution exhibited the slowest rate compared to pH 11.5 and 9.5. However, only when extending incubation to at least one year did the relative depletion rates of different solutions start to align with both the 3-year study by Abdelaal and Rowe (2017) and the current study. Longer incubation times resulted in more accurate depletion rates and, thus, more accurate predictions of antioxidant depletion times.

- The high-load melt index (HLMI) results at 95 and 85 °C suggested consistent degradation by cross-linking in all three solutions. However, data at 75 °C revealed that both chain scission and cross-linking reactions occurred simultaneously and the results were scattered around the initial values after 9.3 years of ageing. While this may imply that the degradation mechanism can change over the range of the experimental temperatures, the GMB exhibited a decrease in all the mechanical properties at the three elevated temperatures in the three high pH solutions. The tensile and SCR properties were more reliable than HLMI in assessing the durations of Stages II and III, as HLMI can be influenced by counteracting mechanisms.
- The break strength and elongation data were used to establish the Arrhenius plots for the duration of Stages II and III. As the pH increased from 9.5 to 13.5, the predicted durations for Stage II increased, while estimates for Stage III slightly decreased. Thus, while pH 13.5 was the most aggressive environment for the GMB based on Std-OIT depletion (Stage I), it was the least aggressive in initiating degradation compared to pH 11.5 and 9.5.
- The t_{NF} predictions for tensile properties based purely on immersion tests were:
 - a- In L6 (pH 9.5) and L7 (pH 11.5): >35 years at 50 °C, >70 years at 40 °C, and >150 years at 30 °C.
 - b- In L8 (pH 13.5): >32 years at 50 °C, >65 years at 40 °C, and >140 years at 30 °C.

Thus, increasing the pH up to 13.5 shortened the GMB's time to nominal failure based on tensile.

- The annealing effect at 95 °C masked the SCR degradation and hence the time nominal failure was established based on 85 and 75 °C. The predicted times to nominal failure ranged from about 8 years at 65 °C, 21 years at 50 °C and more than 80 years at 30 °C. Thus, the predictions are deemed conservative since nominal failure was not reached experimentally at 65 °C. They may be also considered as the worst-case estimates of the time to nominal failure since they were lower than those based on tensile failure.
- Assuming a good liner design that limits the tensile strains in the GMB, based on current knowledge, the time to nominal failure in a composite liner configuration for the geomembrane and solution chemistries examined was estimated to be > 60 years at 50 °C, >260 years at 30 °C, and >1000 years at 10 °C.

Appendix A. Supplementary data

Supplementary data to this article can be found online at <https://doi.org/10.1016/j.geotextmem.2024.09.012>.

Notation

Basic SI units are given in parentheses

A	Pre-exponential factor in the Arrhenius equation (month ⁻¹)
a	Amplitude of the exponential decay function (unitless)
b	Amplitude of the exponential decay function (unitless)
E_a	Activation energy (kJ/mol)
ϵ_B	Percent elongation at break (%)
ϵ_{B0}	Initial percent elongation at break (%)
F_B	Tensile strength at break (kN/m)
F_{B0}	Initial tensile strength at break (kN/m)
$HLMI_0$	Initial High Load Melt Index value
k	Rate of the reaction or degradation process (month ⁻¹)
SCR_m	Stabilized stress-crack resistance after physical ageing (hours)
s	Single antioxidant depletion rate (month ⁻¹)
s_1	Early-time depletion rate (month ⁻¹)
s_2	Later-time depletion rate (month ⁻¹)
OIT_0	Initial OIT value (min)

Competing interests

The authors declare there are no competing interests.

Data

Some or all data used are available from the corresponding author by request.

CRediT authorship contribution statement

Rodrigo A. e Silva: Writing – original draft, Validation, Investigation, Formal analysis, Data curation. **Fady B. Abdelaal:** Writing – review & editing, Supervision, Project administration, Methodology, Investigation, Formal analysis, Data curation, Conceptualization. **R. Kerry Rowe:** Writing – review & editing, Validation, Supervision, Resources, Project administration, Methodology, Investigation, Funding acquisition, Formal analysis, Data curation, Conceptualization.

Data availability

Data will be made available on request.

Acknowledgments

The research presented in this paper was funded by the Natural Science and Engineering Research Council of Canada (NSERC) through an NSERC Discovery Grant to RK Rowe and strategic partnership grant (STPGP 521237) to Rowe, Abdelaal and Brachman, and used equipment provided by funding from the Canada Foundation for Innovation (CFI) and the Ontario Ministry of Research and Innovation. The authors are grateful to their industrial partners, Solmax, Terraflux Geosynthetics Inc., Layfield, Wood, Golder Associates Ltd., Knight-Piesold, Titan Environmental Containment, SNC-Lavalin, Klohn Crippen Berger and the CTT group for their participation in, and contributions to, the overarching project. The authors also acknowledge the contribution of the Coordination for the Improvement of Higher Education Personnel (CAPES, Brazil, Finance Code 001) for partially funding Mr. E Silva. However, the opinions expressed in this paper are solely those of the authors.

OIT_r	Residual OIT value (min)
OIT_t	OIT value at any time t after ageing (min)
R	Universal gas constant ($8.314 \text{ J mol}^{-1} \text{ K}^{-1}$)
T	Temperature (K in the Arrhenius equation)
t	Incubation time (months)
t_d	Predicted time for depletion (months or years)
t_{NF} (or Δt_{NF})	Time to nominal failure (months or years)
Δt_{II}	Length of Stage II
Δt_{III}	Length of Stage III
η	Degradation rate of the GMB tensile property of interest during Stage II
γ	Degradation rate of the GMB tensile property of interest during Stage III

ABBREVIATIONS

ASTM	American Society for Testing and Materials
GMB	Geomembrane
GRI	Geosynthetic Research Institute
HALS	Hindered Amines Stabilizers
HLMI	High Load Melt Index
HDPE	High-density Polyethylene
HP-OIT	High-pressure Oxidative Induction Time
MSW	Municipal Solid Waste
NaOH	Sodium Hydroxide
NCTL-SCR	Notched Constant Tensile Load Stress-crack Resistance
OIT	Oxidative Induction Time
PLS	Pregnant Liquor Solution
SCR	Stress-crack Resistance
Std-OIT	Standard Oxidative Induction Time
XD	Cross-machine Direction

References

- Abdelaal, F.B., Morsy, M.S., Rowe, R.K., 2019. Long-term performance of a HDPE geomembrane stabilized with HALS in chlorinated water. *Geotext. Geomembranes* 47 (6), 815–830. <https://doi.org/10.1016/j.geotextmem.2019.103497>.
- Abdelaal, F.B., Rowe, R.K., 2017. Effect of high pH found in low-level radioactive waste leachates on the antioxidant depletion of a HDPE geomembrane. *Journal of Hazardous, Toxic, and Radioactive Waste* 21 (1), 1–15. [https://doi.org/10.1061/\(ASCE\)HZ.2153-5515.0000262](https://doi.org/10.1061/(ASCE)HZ.2153-5515.0000262).
- Abdelaal, F.B., Rowe, R.K., 2014a. Effect of high temperatures on antioxidant depletion from different HDPE geomembranes. *Geotext. Geomembranes* 42 (4), 284–301. <https://doi.org/10.1016/j.geotextmem.2014.05.002>.
- Abdelaal, F.B., Rowe, R.K., 2014b. Application of a four-parameter exponential decay model for modelling antioxidant depletion in HDPE geomembranes. In: 10th International Conference on Geosynthetics, ICG 2014. International Geosynthetics Society, Berlin, Germany, pp. 1–9.
- Abdelaal, F.B., Rowe, R.K., 2023. Physical and mechanical performance of a HDPE Geomembrane in ten mining solutions with different pHs. *Can. Geotech. J.* 60 (7), 978–993. <https://doi.org/10.1139/cgj-2022-0419>.
- Abdelaal, F.B., Rowe, R.K., Brachman, R.W.I., 2014a. Brittle rupture of an aged HDPE geomembrane at local gravel indentations under simulated field conditions. *Geosynth. Int.* 21 (1), 1–23. <https://doi.org/10.1680/gein.13.00031>.
- Abdelaal, F.B., Rowe, R.K., Hsuan, Y.G., Awad, R., 2015. Effect of high temperatures on the physical and mechanical properties of HDPE geomembranes in air. *Geosynth. Int.* 22 (3), 207–224. <https://doi.org/10.1680/gein.15.00006>.
- Abdelaal, F.B., Rowe, R.K., Islam, M.Z., 2014b. Effect of leachate composition on the long-term performance of a HDPE geomembrane. *Geotext. Geomembranes* 42, 348–362. <https://doi.org/10.1016/j.geotextmem.2014.06.001>.
- Abdelaal, F.B., Rowe, R.K., Morsy, M.S., e Silva, R.A., 2023. Degradation of HDPE, LLDPE, and blended polyethylene geomembranes in extremely low and high pH mining solutions at 85 °C. *Geotext. Geomembranes* 51 (5), 27–38. <https://doi.org/10.1016/j.geotextmem.2023.04.011>.
- Al-Malika, S., 2004. Perspectives in stabilisation of polyolefins. In: *Long Term Properties of Polyolefins*, first ed. Springer, Verlag, Heidelberg, Germany, pp. 121–150.
- Ancheyta, J., 2017. Fundamentals of chemical reaction kinetics. In: *Chemical Reaction Kinetics: Concepts, Methods and Case Studies*, first ed. John Wiley and Sons Ltd, pp. 1–53.
- Asamoah, R.K., Skinner, W., Addai-Mensah, J., 2018. Alkaline cyanide leaching of refractory gold flotation concentrates and bio-oxidised products: the effect of process variables. *Hydrometallurgy* 179, 79–93. <https://doi.org/10.1016/j.hydromet.2018.05.010>.
- ASTM D1238, 2020. Standard Test Method for Melt Flow Rates of Thermoplastics by Extrusion Plastometer. American Society for Testing and Materials, West Conshohocken, Pennsylvania, USA.
- ASTM D3895, 2019. Standard Test Method for Oxidative-Induction Time of Polyolefins by Differential Scanning Calorimetry. American Society for Testing and Materials, West Conshohocken, Pennsylvania, USA.
- ASTM D5322, 2023. Standard Practice for Laboratory Immersion Procedures for Evaluating the Chemical Resistance of Geosynthetics to Liquids. American Society for Testing and Materials, West Conshohocken, Pennsylvania, USA.
- ASTM D5397, 2019. Standard Test Method for Evaluation of Stress Crack Resistance of Polyolefin Geomembranes Using Notched Constant Tensile Load Test. American Society for Testing and Materials, West Conshohocken, Pennsylvania, USA.
- ASTM D5885, 2020. Standard Test Method for Oxidative Induction Time of Polyolefin Geosynthetics by High-Pressure Differential Scanning Calorimetry. American Society for Testing and Materials, West Conshohocken, Pennsylvania, USA.
- ASTM D6693, 2020. Standard Test Method for Determining Tensile Properties of Nonreinforced Polyethylene and Nonreinforced Flexible Polypropylene Geomembranes. American Society for Testing and Materials, West Conshohocken, Pennsylvania, USA.
- Breitenbach, A.J., Smith, M.E., 2006. Overview of geomembrane history in the mining industry. In: *Proceedings of the 8th International Conference on Geosynthetics Society*. International Geosynthetics Society, Yokohama, Japan, pp. 1–4.
- Brown, N., Lu, X., Huang, Y., Qian, R., 1991. Slow crack growth in polyethylene - a review. *Makromol. Chem. Macromol. Symp.* 41, 55–67.
- Celina, M., Gillen, K.T., Clough, R.L., 1998. Inverse temperature and annealing phenomena during degradation of crosslinked polyolefins. *Polym. Degrad. Stabil.* 61 (2), 231–244. [https://doi.org/10.1016/S0141-3910\(97\)00142-0](https://doi.org/10.1016/S0141-3910(97)00142-0).
- Clinton, M., Rowe, R.K., 2023. Antioxidant-stabilizer depletion of 4 HDPE geomembranes with high HP-OIT in MSW leachate. *Geosynth. Int.* <https://doi.org/10.1680/jgein.23.00041> (Ahead of Print).
- E Silva, R.A., Abdelaal, F.B., Rowe, R.K., 2021. Antioxidant depletion of a HDPE geomembrane in arsenic-bearing tailings. In: *Proceedings of the 74th Canadian Geotechnical Conference*. Canadian Geotechnical Society, Niagara Falls, Canada, pp. 1–5.
- E Silva, R.A., Abdelaal, F.B., Rowe, R.K., 2022. Antioxidant depletion from a HDPE geomembrane immersed in unsaturated tailings pore waters and heap leaching solutions. In: *Proceedings of the 75th Canadian Geotechnical Conference*. Canadian Geotechnical Society, Calgary (Canada), pp. 1–6.
- E Silva, R.A., Morsy, M.S., Abdelaal, F.B., Rowe, R.K., 2023. Comparison between the environmental stress-crack resistance of unaged and aged HDPE and LLDPE geomembranes. In: *Proceedings of the 12th International Conference on Geosynthetics*. International Geosynthetics Society, Rome (Italy), pp. 753–759.
- Espitia, S.L.M., Lapidus, G.T., 2015. Pretreatment of a refractory arsenopyritic gold ore using hydroxyl ion. *Hydrometallurgy* 153, 106–113. <https://doi.org/10.1016/j.hydromet.2015.02.013>.
- Ewais, A.M.R., Rowe, R.K., 2014. Effect of aging on the stress crack resistance of an HDPE geomembrane. *Polym. Degrad. Stabil.* 109, 194–208. <https://doi.org/10.1016/j.polymdegradstab.2014.06.013>.

- Ewais, A.M.R., Rowe, R.K., Rimal, S., Sangam, H.P., 2018. 17-year elevated temperature study of HDPE geomembrane longevity in air, water and leachate. *Geosynth. Int.* 25 (5). <https://doi.org/10.1680/jgein.18.00016>.
- Ewais, A.M.R., Rowe, R.K., Scheirs, J., 2014. Degradation behaviour of HDPE geomembranes with high and low initial high-pressure oxidative induction time. *Geotext. Geomembranes* 42 (2), 111–126. <https://doi.org/10.1016/j.geotextmem.2014.01.004>.
- Ghorbani, Y., Franzidis, J.P., Petersen, J., 2016. Heap leaching technology - current state, innovations, and future directions: a review. *Miner. Process. Extr. Metall. Rev.* 37 (2), 73–119. <https://doi.org/10.1080/08827508.2015.1115990>.
- Grause, G., Chien, M.F., Inoue, C., 2020. Changes during the weathering of polyolefins. *Polym. Degrad. Stabil.* 181, 109364. <https://doi.org/10.1016/j.polymdegradstab.2020.109364>.
- GRI (Geosynthetic Research Institute), 2021. Standard specification for test methods, test properties and testing frequency for high density polyethylene (HDPE) smooth and textured geomembranes. In: GRI Test Method Geomembrane 13. Geosynthetic Research Institute, Folsom, Pennsylvania, USA.
- Gulec, S.B., Benson, C.H., Edil, T.B., 2005. Effect of acidic mine drainage on the mechanical and hydraulic properties of three geosynthetics. *J. Geotech. Geoenviron. Eng.* 131, 937–950. [https://doi.org/10.1061/\(ASCE\)1090-0241\(2005\)131:8\(937\)](https://doi.org/10.1061/(ASCE)1090-0241(2005)131:8(937)).
- Gulec, S.B., Edil, T.B., Benson, C.H., 2004. Effect of acidic mine drainage on the polymer properties of an HDPE geomembrane. *Geosynth. Int.* 11 (2), 60–72. <https://doi.org/10.1680/jgein.2004.11.2.60>.
- Hsuan, Y.G., Koerner, R.M., 1998. Antioxidant depletion lifetime in high density polyethylene geomembranes. *J. Geotech. Geoenviron. Eng.* 124 (6), 532–541. [https://doi.org/10.1061/\(ASCE\)1090-0241\(1998\)124:6\(532\)](https://doi.org/10.1061/(ASCE)1090-0241(1998)124:6(532)).
- Jeon, H.Y., Bouazza, A., Lee, K.Y., 2008. Depletion of antioxidants from an HDPE geomembrane upon exposure to acidic and alkaline solutions. *Polym. Test.* 27 (4), 434–440. <https://doi.org/10.1016/j.polymtest.2008.01.003>.
- Koontz, J.L., Marcy, J.E., O'Keefe, S.F., Duncan, S.E., Long, T.E., Moffitt, R.D., 2010. Polymer processing and characterization of LLDPE films loaded with α -tocopherol, quercetin, and their cyclodextrin inclusion complexes. *J. Appl. Polym. Sci.* 117 (4), 2299–2309. <https://doi.org/10.1002/app.32044>.
- Kutz, M., 2018. *Handbook of Environmental Degradation of Materials*, third ed. William Andrew.
- Laidler, K.J., 1984. The development of the Arrhenius equation. *J. Chem. Educ.* 61 (6), 494–498. <https://doi.org/10.1021/ed061p494>.
- Laidler, K.J., 1987. *Theory of reaction rates*. In: *Chemical Kinetics*, third ed. Pearson, pp. 80–136.
- Lavoie, F.L., Kobelnik, M., Valentin, C.A., Fernanda, É., Lopes, M.D.L., Lins, J., 2021. Environmental protection with HDPE geomembranes in mining facility constructions. *Construction Materials* 1, 122–133. <https://doi.org/10.3390/constrmater1020009>.
- Li, W., Xu, Y., Huang, Q., Liu, Y., Liu, J., 2021. Antioxidant depletion patterns of high-density polyethylene geomembranes in landfills under different exposure conditions. *Waste Manag.* 121, 365–372. <https://doi.org/10.1016/j.wasman.2020.12.025>.
- Likozar, B., Krajnc, M., 2011. Cross-linking of polymers: kinetics and transport phenomena. *Ind. Eng. Chem. Res.* 50 (3), 1558–1570. <https://doi.org/10.1021/ie1015415>.
- Lu, X., Qian, R., McGhie, A.R., Brown, N., 1992. The effect of annealing on slow crack growth in an ethylene-hexene copolymer. *J. Polym. Sci. B Polym. Phys.* 30, 899–906. <https://doi.org/10.1002/polb.1995.090330116>.
- Lupo, J.F., 2010. Liner system design for heap leach pads. *Geotext. Geomembranes* 28 (2), 163–173. <https://doi.org/10.1016/j.geotextmem.2009.10.006>.
- Lupo, J.F., Morrison, K.F., 2007. Geosynthetic design and construction approaches in the mining industry. *Geotext. Geomembranes* 25 (2), 96–108. <https://doi.org/10.1016/j.geotextmem.2006.07.003>.
- Manning, T.J., Kappes, D.W., 2016. Heap leaching of gold and silver ores. In: *Gold Ore Processing*, second ed. Elsevier B.V., pp. 413–428.
- McDonnell, D., Balfe, N., O'Donnell, G.E., 2017. Chemical ageing effects on the mechanical behaviour of ethylene-propylene diene monomer. *Polym. Test.* 64, 167–174. <https://doi.org/10.1016/j.polymtest.2017.10.001>.
- Melashvili, M., Fleming, C., Dymov, I., Matthews, D., Dreisinger, D., 2016. Dissolution of gold during pyrite oxidation reaction. *Miner. Eng.* 87, 2–9. <https://doi.org/10.1016/j.mineng.2015.07.017>.
- Menzinger, M., Wolfgang, R., 1969. The meaning and use of the Arrhenius activation energy. *Angew. Chem. Int. Ed. Engl.* 8 (6), 438–444. <https://doi.org/10.1002/anie.196904381>.
- Morsy, M.S., Rowe, R.K., 2020. Effect of texturing on the longevity of high-density polyethylene (HDPE) geomembranes in municipal solid waste landfills. *Can. Geotech. J.* 57 (1), 61–72. <https://doi.org/10.1139/cgj-2019-0047>.
- Morsy, M.S., Rowe, R.K., Abdelaal, F.B., 2021. Longevity of twelve geomembranes in chlorinated water. *Can. Geotech. J.* 58 (479–495), 1–52. <https://doi.org/10.1139/cgj-2019-0520>.
- Müller, W.W., 2010. *HDPE Geomembranes in Geotechnics*, first ed. Springer, Verlag, Heidelberg, Germany.
- Müller, W.W., Jakob, I., Tatzky-Gerth, R., Wohlecke, A., 2016. A study on antioxidant depletion and degradation in polyolefin-based geosynthetics: sacrificial versus regenerative stabilization. *Polym. Eng. Sci.* 56 (2), 129–142. <https://doi.org/10.1002/pen.24199>.
- Oraby, E.A., Eksteen, J.J., 2016. Gold dissolution and copper suppression during leaching of copper-gold gravity concentrates in caustic soda-low free cyanide solutions. *Miner. Eng.* 87, 10–17. <https://doi.org/10.1016/j.mineng.2015.08.006>.
- Peterlin, A., 1975. Dependence of diffusive transport on morphology of crystalline polymers. *J. Macromol. Sci., Part B: Phys.* 11 (1), 57–87. <https://doi.org/10.1080/00222347508217855>.
- Petersen, J., 2016. Heap leaching as a key technology for recovery of values from low-grade ores – a brief overview. *Hydrometallurgy* 165, 206–212. <https://doi.org/10.1016/j.hydromet.2015.09.001>.
- Pries, J., Bishop, D., Hayes, S., 2014. The use of geosynthetics in mining works. In: *Proceedings of the 20th WasteCon Conference*. Institute of Waste Management of Southern Africa, Johannesburg, Gauteng, South Africa, pp. 189–194.
- Pyper, R., Seal, T., Uhrig, J.L., Miller, G.C., 2019. *Dump and heap leaching*. In: *SME Mineral Processing and Extractive Metallurgy Handbook*, first ed. Society for Mining, Metallurgy, and Exploration, Englewood, Colorado (USA), pp. 1207–1224.
- Robertson, S.W., van Staden, P.J., Cherkayev, A., Petersen, J., 2022. Properties governing the flow of solution through crushed ore for heap leaching. *Hydrometallurgy* 208. <https://doi.org/10.1016/j.hydromet.2021.105811>.
- Roe, R.J., Bair, H.E., Gieniewski, C., 1974. Solubility and diffusion coefficient of antioxidants in polyethylene. *J. Appl. Polym. Sci.* 18 (3), 843–856. <https://doi.org/10.1002/app.1974.070180319>.
- Rowe, R.K., Abdelaal, F.B., 2016. Antioxidant depletion in HDPE geomembrane with HALS in low pH heap leach environment. *Can. Geotech. J.* 53, 1612–1627. <https://doi.org/10.1139/cgj-2016-0026>.
- Rowe, R.K., Abdelaal, F.B., Islam, M.Z., 2014. Aging of high-density polyethylene geomembranes of three different thicknesses. *J. Geotech. Geoenviron. Eng.* 140 (5), 1–11. [https://doi.org/10.1061/\(asce\)gt.1943-5606.0001090](https://doi.org/10.1061/(asce)gt.1943-5606.0001090).
- Rowe, R.K., Abdelaal, F.B., Zafari, M., Morsy, M.S., Priyanto, D.G., 2020. An approach to high-density polyethylene (HDPE) geomembrane selection for challenging design requirements. *Can. Geotech. J.* 57 (10), 1550–1565. <https://doi.org/10.1139/cgj-2019-0572>.
- Rowe, R.K., Brachman, R.W.I., Irfan, H., Smith, M.E., Thiel, R., 2013. Effect of underliner on geomembrane strains in heap leach applications. *Geotext. Geomembranes* 40, 37–47. <https://doi.org/10.1016/j.geotextmem.2013.07.009>.
- Rowe, R.K., Ewais, A.M.R., 2014. Antioxidant depletion from five geomembranes of same resin but of different thicknesses immersed in leachate. *Geotext. Geomembranes* 42 (5), 540–554. <https://doi.org/10.1016/j.geotextmem.2014.08.001>.
- Rowe, R.K., Islam, M.Z., Hsuan, Y.G., 2010. Effects of thickness on the aging of HDPE geomembranes. *J. Geotech. Geoenviron. Eng.* 136 (2), 299–309. [https://doi.org/10.1061/\(ASCE\)GT.1943-5606.0000207](https://doi.org/10.1061/(ASCE)GT.1943-5606.0000207).
- Rowe, R.K., Islam, M.Z., Hsuan, Y.G., Islam, M.Z., Hsuan, Y.G., 2008. Leachate chemical composition effects on OIT depletion in an HDPE geomembrane. *Geosynth. Int.* 15 (2), 136–151. <https://doi.org/10.1680/jgein.2008.15.2.136>.
- Rowe, R.K., Morsy, M.S., Ewais, A.M.R., 2019. Representative stress crack resistance of polyolefin geomembranes used in waste management. *Waste Manag.* 100, 18–27. <https://doi.org/10.1016/j.wasman.2019.08.028>.
- Rowe, R.K., Quigley, R.M., Brachman, R.W.I., Booker, J.R., 2004. *Barrier Systems for Waste Disposal Facilities*, second ed. CRC Press Taylor & Francis Group, Boca Raton, FL.
- Rowe, R.K., Rimal, S., Sangam, H., 2009. Ageing of HDPE geomembrane exposed to air, water and leachate at different temperatures. *Geotext. Geomembranes* 27, 137–151. <https://doi.org/10.1016/j.geotextmem.2008.09.007>.
- Rowe, R.K., Sangam, H.P., 2002. Durability of HDPE geomembranes. *Geotext. Geomembranes* 20, 77–95. [https://doi.org/10.1016/S0266-1144\(02\)00005-5](https://doi.org/10.1016/S0266-1144(02)00005-5).
- Rowe, R.K., Shoaib, M., 2017. Long-term performance of high-density polyethylene (HDPE) geomembrane seams in municipal solid waste (MSW) leachate. *Can. Geotech. J.* 54 (12), 1623–1636. <https://doi.org/10.1139/cgj-2017-0049>.
- Sangam, H.P., Rowe, R.K., 2002. Effects of exposure conditions on the depletion of antioxidants from high-density polyethylene (HDPE) geomembranes. *Can. Geotech. J.* 39 (6), 1221–1230. <https://doi.org/10.1139/t02-074>.
- Scheirs, J., 2009. *A Guide to Polymeric Geomembranes: a Practical Approach*, first ed. John Wiley and Sons Ltd, Chichester, UK.
- Schlotter, N.E., Furlan, P.Y., 1992. A review of small molecule diffusion in polyolefins. *Polymer* 33 (16), 3323–3342. [https://doi.org/10.1016/0032-3861\(92\)91089-K](https://doi.org/10.1016/0032-3861(92)91089-K).
- Schmidt, G., Malwitz, M.M., 2003. Properties of polymer-nanoparticle composites. *Curr. Opin. Colloid Interface Sci.* 8 (1), 103–108. [https://doi.org/10.1016/S1359-0294\(03\)00008-6](https://doi.org/10.1016/S1359-0294(03)00008-6).
- Schrauwen, B.A.G., Janssen, R.P.M., Govaert, L.E., Meijer, H.E.H., 2004. Intrinsic deformation behavior of semicrystalline polymers. *Macromolecules* 37 (16), 6069–6078. <https://doi.org/10.1021/ma035279t>.
- Seeger, S., Müller, W., 2003. Theoretical approach to designing protection: selecting a geomembrane strain criterion. In: *Geosynthetics: Protecting the Environment*. Thomas Telford, London, pp. 137–152.
- Snyders, C.A., Akdogan, G., Bradshaw, S.M., van Vreden, J.H., Smith, R., 2018. The development of a caustic pre-leaching step for the recovery of Au from a refractory ore tailings heap. *Miner. Eng.* 121, 23–30. <https://doi.org/10.1016/j.mineng.2018.02.014>.
- Thenepalli, T., Chilakala, R., Habte, L., Tuan, L.Q., Kim, C.S., 2019. A brief note on the heap leaching technologies for the recovery of valuable metals. *Sustainability* 11 (12). <https://doi.org/10.3390/su10023347>.
- Thiel, R., Smith, M.E., 2004. State of the practice review of heap leach pad design issues. *Geotext. Geomembranes* 22 (6), 555–568. <https://doi.org/10.1016/j.geotextmem.2004.05.002>.
- Yang, X., Rozelle, P.L., Pisupati, S.V., 2021. The effect of caustic soda treatment to recover rare earth elements from secondary feedstocks with low concentrations. *Miner. Eng.* 173, 107184. <https://doi.org/10.1016/j.mineng.2021.107184>.
- Zafari, M., Abdelaal, F.B., Rowe, R.K., 2023a. Long-term performance of conductive-backed multilayered HDPE geomembranes. *Geotext. Geomembranes* 51 (4), 137–155. <https://doi.org/10.1016/j.geotextmem.2023.03.007>.

- Zafari, M., Abdelaal, F.B., Rowe, R.K., 2023b. Degradation behavior of two multilayered textured white HDPE geomembranes and their smooth edges. *J. Geotech. Geoenviron. Eng.* 149 (5), 1–15. <https://doi.org/10.1061/jggefek.gteng-11101>.
- Zafari, M., Rowe, R.K., Abdelaal, F.B., 2023c. Longevity of multilayered textured HDPE geomembranes in low-level waste applications. *Can. Geotech. J.* 1–36. <https://doi.org/10.1139/cgj-2023-0039>.

- Zeiner, T., Fischlschweiger, M., 2023. Diffusion and transport through nanoscale polymer-based coatings. In: *Polymer-Based Nanoscale Materials for Surface Coatings*, first ed. Elsevier, pp. 291–321.